

## 1 InGaAs/GaAs PIN photodiodes

- 1-1 Characteristics
- 1-2 How to use

## 2 InGaAs APD

- 2-1 Operating principle
- 2-2 Characteristics
- 2-3 How to use

## 3 ROSA modules

- 3-1 Structure
- 3-2 Features
- 3-3 Characteristics
- 3-4 Precautions

## 4 PbS/PbSe photoconductive detectors

- 4-1 Operating principle
- 4-2 Characteristics
- 4-3 How to use

## 5 InSb photoconductive detectors

## 6 InAs/InAsSb/InSb photovoltaic detectors

- 6-1 Characteristics
- 6-2 Precautions

## 7 MCT (HgCdTe) photoconductive detectors

- 7-1 Characteristics
- 7-2 How to use

## 8 MCT (HgCdTe) photovoltaic detectors

- 8-1 Characteristics
- 8-2 How to use

## 9 Two-color detectors

## 10 Options

## 11 New approaches

- 11-1 High-speed InGaAs PIN photodiodes
- 11-2 100 Gbps ROSA modules
- 11-3 InAsSb photovoltaic detectors

## 12 Applications

- 12-1 Optical power meters
- 12-2 LD monitors
- 12-3 Radiation thermometers
- 12-4 Distance measurement
- 12-5 Flame eyes (flame monitors)
- 12-6 Moisture meters
- 12-7 Gas analyzers
- 12-8 Infrared imaging devices
- 12-9 Remote sensing
- 12-10 Sorting machines
- 12-11 FT-IR

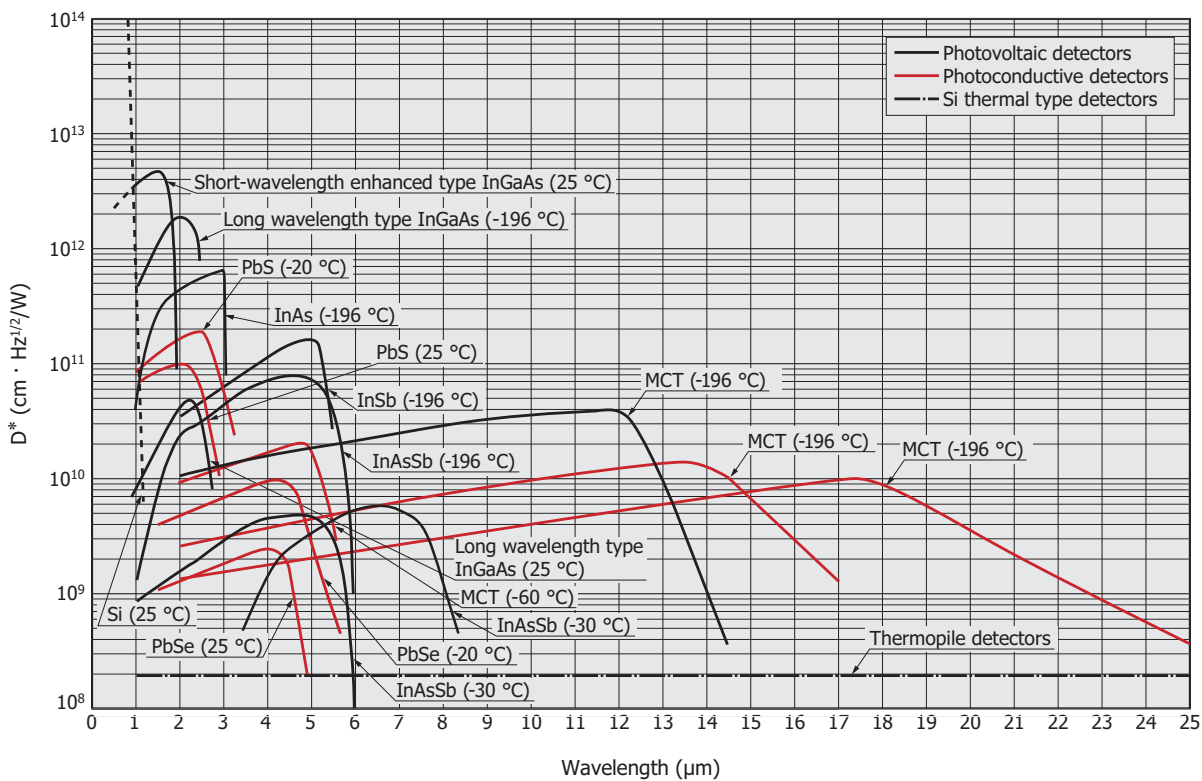
# Compound semiconductor photosensors



Compound semiconductor photosensors are opto-semiconductors made of two or more elements mainly from groups II to VI. These photosensors have different spectral response ranges depending on the elements comprising them. This means photosensors can be made that are sensitive to different wavelengths from the ultraviolet to infrared region.

Hamamatsu provides detectors for many different wavelengths by taking advantage of its expertise in compound semiconductor technology accumulated over many years. We offer an especially wide detector product lineup in the infrared region. Applications for our compound semiconductor photosensors range from academic research to information communication devices and general-purpose electronic equipment.

## Spectral response of compound semiconductor photosensors (typical example)



KIRD80259EJ

## Hamamatsu compound semiconductor photosensors

Product name	Spectral response range (μm)				Features
	0	1	2	3	
InGaAs PIN photodiode	0.5 — 1.7				<ul style="list-style-type: none"> <li>Short-wavelength enhanced type</li> <li>Can detect light from 0.5 μm</li> </ul>
	0.9 — 1.7				<ul style="list-style-type: none"> <li>Standard type</li> <li>High-speed response, high sensitivity, low dark current</li> <li>Various types of photosensitive areas, arrays, and packages available</li> </ul>
	0.9 — 1.9				<ul style="list-style-type: none"> <li>For light measurement around 1.7 μm</li> <li>TE-cooled type available</li> </ul>
	0.9 — 2.1				<ul style="list-style-type: none"> <li>For light measurement in water absorption band (1.9 μm)</li> <li>TE-cooled type available</li> </ul>
InGaAs APD	0.9 — 2.6				<ul style="list-style-type: none"> <li>For NIR spectrometry</li> <li>TE-cooled type available</li> </ul>
	0.95 — 1.7				<ul style="list-style-type: none"> <li>High sensitivity, high-speed response, low capacitance, low dark current</li> <li>Various sizes of photosensitive areas available</li> </ul>
GaAs PIN photodiode	0.57 0.87				<ul style="list-style-type: none"> <li>High-speed response, high sensitivity, low dark current</li> <li>Arrays and various packages available</li> </ul>

Product name	Spectral response range (μm)						Features
	0	5	10	15	20	25	
PbS photoconductive detector	1 3.2						<ul style="list-style-type: none"> <li>Photoconductive detectors whose resistance decreases with input of infrared light</li> <li>Can be used at room temperatures in a wide range of applications such as radiation thermometers and flame monitors</li> </ul>
PbSe photoconductive detector	1 5.2						<ul style="list-style-type: none"> <li>Detects wavelengths up to 5.2 μm</li> <li>Offers higher response speed at room temperatures compared to other detectors used in the same wavelength range. Suitable for a wide range of applications such as gas analyzers.</li> </ul>
InAs photovoltaic detector	1 3.8						<ul style="list-style-type: none"> <li>Covers a spectral response range close to PbS but offers higher response speed</li> </ul>
InAsSb photovoltaic detector	1 5.8						<ul style="list-style-type: none"> <li>High-sensitivity, high-reliability Infrared detector for the 8 μm band</li> <li>High-speed response</li> </ul>
InSb photoconductive detector	1 6.7						<ul style="list-style-type: none"> <li>Detects wavelengths up to around 6.5 μm, with high sensitivity over long periods of time by thermoelectric cooling</li> </ul>
InSb photovoltaic detector	1 5.5						<ul style="list-style-type: none"> <li>High sensitivity in so-called atmospheric window (3 to 5 μm)</li> <li>High-speed response</li> </ul>
MCT (HgCdTe) photoconductive detector	1 — 25						<ul style="list-style-type: none"> <li>Various types with different spectral response ranges are provided by changing the HgTe and CdTe composition ratio.</li> <li>High-sensitivity photoconductive detectors whose resistance decreases with input of infrared light</li> <li>Thermoelectric cooled type and cryogenic dewars available</li> </ul>
MCT (HgCdTe) photovoltaic detector	1 — 13.5						<ul style="list-style-type: none"> <li>High-speed response, low noise</li> </ul>
Two-color detector	Si + PbS 0.2 3						<ul style="list-style-type: none"> <li>Wide spectral response range</li> <li>Incorporates two photosensors with different spectral response ranges on top of each other on the same optical axis</li> </ul>
	Si + PbSe 0.2 4.85						
	Si + InGaAs 0.32 2.55						
	Standard type InGaAs + long wavelength type InGaAs 0.9 2.55						
Photon drag detector	10						<ul style="list-style-type: none"> <li>High-speed detector with sensitivity in 10 μm band (for CO<sub>2</sub> laser detection)</li> <li>Room temperature operation with high-speed response</li> </ul>

## Hamamatsu optical communication detectors

Product name	Wavelength	Transmission bandwidth (frequency)	Package style			
			Metal	Receptacle	Pigtail	ROSA
InGaAs PIN photodiode	1.3/1.55 μm	(2 GHz)	—			—
InGaAs PIN photodiode with preamp		2.5 Gbps				—
		10 Gbps	—	—	—	

Note: The following optical communication devices are also available.

· Photodiodes for monitoring light level and wavelength

InGaAs PIN photodiodes (metal type, bare chip type, sub-mount type)

InGaAs PIN photodiode arrays, InGaAs linear image sensors

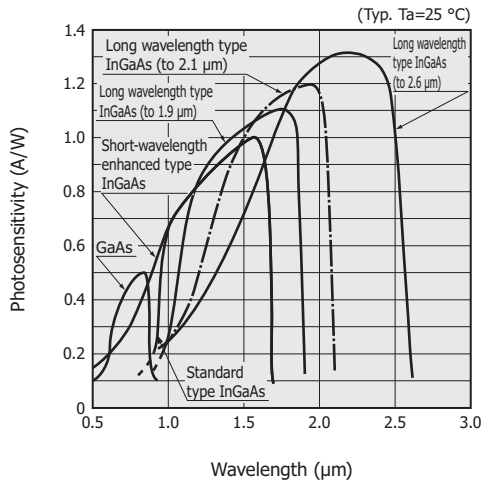
· Photodiodes, infrared LED, and photo IC for optical link

· Photodiodes and infrared LED for FSO (free space optics), light emitting/receiving module for VICS (Vehicle Information and Communication System) on vehicle

# 1. InGaAs/GaAs PIN photodiodes

InGaAs PIN photodiodes and GaAs PIN photodiodes are photovoltaic detectors having PN junction just the same as Si photodiodes.

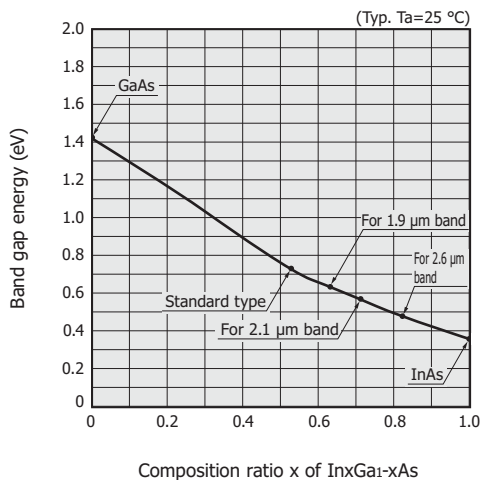
[Figure 1-1] Spectral response (InGaAs/GaAs PIN photodiodes)



KIRDB0332EE

InGaAs has a smaller band gap energy compared to Si, so it is sensitive to longer wavelengths. Since the InGaAs band gap energy varies depending on the composition ratio of In and Ga [Figure 1-2], infrared detectors with different spectral response ranges can be fabricated by just changing this composition ratio. Hamamatsu provides standard types having a cutoff wavelength of 1.7 μm, short-wavelength enhanced types, and long wavelength types having a cutoff wavelength extending to 1.9 μm or 2.1 μm or up to 2.6 μm.

[Figure 1-2] Band gap energy vs. composition ratio x of In<sub>x</sub>Ga<sub>1-x</sub>As



KIRDB0130EB

## 1-1 Characteristics

### Current vs. voltage characteristics

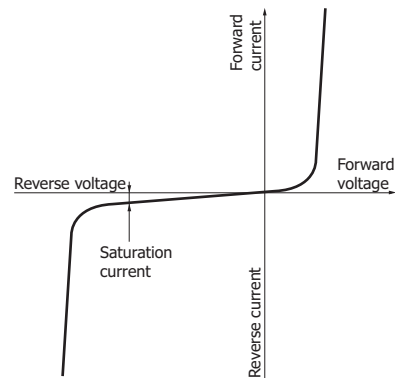
When voltage is applied to an InGaAs/GaAs PIN photodiode in a dark state, current vs. voltage characteristics like that shown in Figure 1-3 (a) are obtained. When light enters the photodiode, this curve shifts as shown at ② in Figure 1-3 (b). As the light level is increased, the curve further shifts as shown at ③. Here, when both terminals of the photodiode are left open, an open circuit voltage ( $V_{oc}$ ) appears in the forward direction. When both terminals are shorted, a short circuit current ( $I_{sc}$ ) flows in the reverse direction.

Figure 1-4 shows methods for measuring the light level by detecting the photocurrent. In Figure 1-4 (a), a load resistor is connected and the voltage  $I_o \times R_L$  is amplified by an amplifier having a gain of  $G$ . In this circuit, the linearity range is limited [Figure 1-3 (c)].

Figure 1-4 (b) shows a circuit connected to an op amp. If we set the open-loop gain of the op amp as  $A$ , then the equivalent input resistance becomes  $R_f/A$  due to negative feedback circuit characteristics. This resistance is several orders of magnitude smaller than the input resistance of the circuit in Figure 1-4 (a), allowing ideal measurement of the short circuit current ( $I_{sc}$ ). If the short circuit current must be measured over a wide range, then change the  $R_f$  as needed.

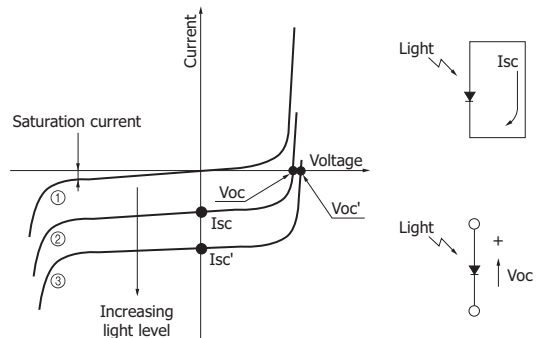
[Figure 1-3] Current vs. voltage characteristics

#### (a) In dark state



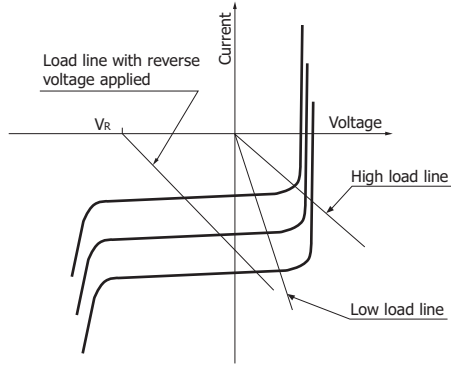
KIRD0030EA

#### (b) When light is incident



KPDC0005EA

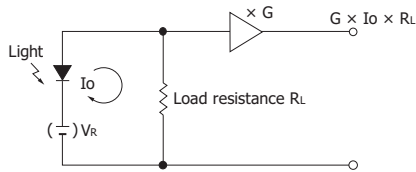
**(c) Current vs. voltage characteristics and load line**



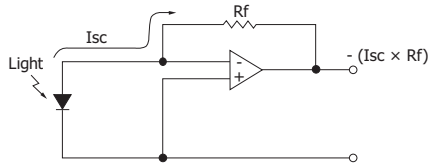
KPDB0003EB

[Figure 1-4] Connection examples

**(a) When load resistor is connected**



**(b) When op amp is connected**



KPDC0006ED

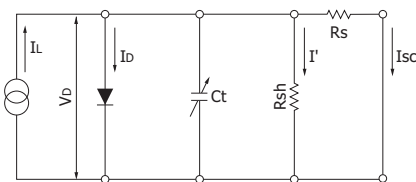
**Equivalent circuit**

A circuit equivalent to an InGaAs/GaAs PIN photodiode is shown in Figure 1-5. The short circuit current ( $I_{sc}$ ) is expressed by equation (1). The linearity limit of the short circuit current is determined by the 2nd and 3rd terms of this equation.

$$I_{sc} = I_L - I_s \left[ \exp \frac{q (I_{sc} \times R_s)}{k T} - 1 \right] - \frac{I_{sc} \times R_s}{R_{sh}} \dots \dots (1)$$

- $I_L$  : current generated by incident light (proportional to light level)
- $I_s$  : photodiode reverse saturation current
- $q$  : electron charge
- $R_s$  : series resistance
- $k$  : Boltzmann's constant
- $T$  : absolute temperature of photodiode
- $R_{sh}$  : shunt resistance

[Figure 1-5] Equivalent circuit (InGaAs/GaAs PIN photodiode)



- $V_o$  : voltage across diode
- $I_o$  : diode current
- $C_t$  : terminal capacitance
- $I'$  : shunt resistance current
- $V_o$  : output voltage
- $I_o$  : output current

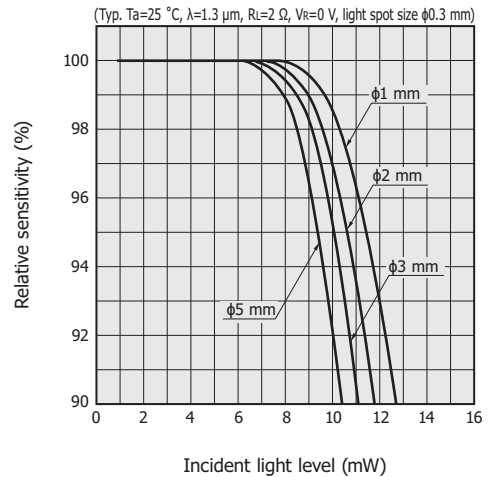
KPDC0004EB

**Linearity**

The lower limit of InGaAs/GaAs PIN photodiode linearity is determined by noise while the upper limit is determined by the chip structure and composition, photosensitive area size, electrode structure, incident light spot size, and the like. To expand the upper limit, a reverse voltage is applied in some cases. However, applying 1 V is sufficient if only the linearity needs to be considered. Figure 1-7 shows connection examples for applying a reverse voltage. Although applying a reverse voltage is useful to improve the linearity or response characteristics, it also results in larger dark current and higher noise level. Excessive reverse voltages might also damage or deteriorate the photodiode, so always use the reverse voltage that is within the absolute maximum rating and set the polarity so that the cathode is at positive potential relative to the anode.

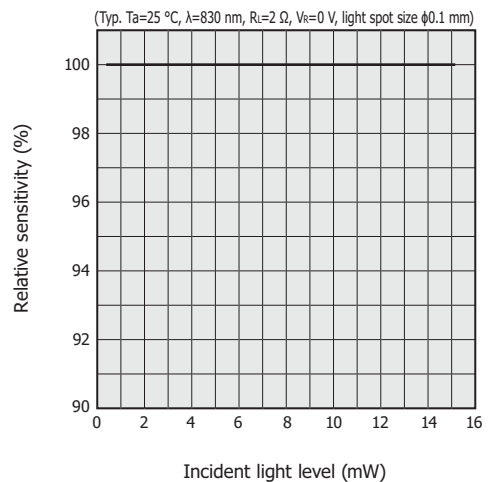
[Figure 1-6] Linearity

**(a) InGaAs PIN photodiodes**



KIRD00333EB

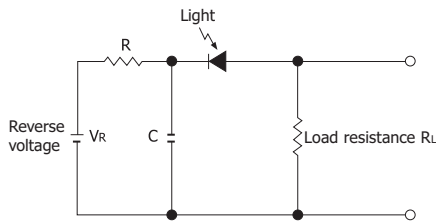
**(b) GaAs PIN photodiode**



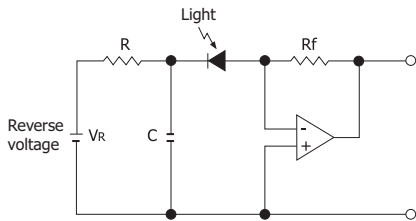
KGPDB0060EA

[Figure 1-7] Connection examples  
(with reverse voltage applied)

(a) When load resistor is connected



(b) When op amp is connected



KPDC008EB

### □ Noise characteristics

Like other typical photosensors, the lower limits of light detection for InGaAs/GaAs PIN photodiodes are determined by their noise characteristics. Noise current ( $i_n$ ) in a photodiode is the sum of the thermal noise current (or Johnson noise current)  $i_j$  of a resistor, which approximates the shunt resistance  $R_{sh}$ , and the shot noise currents  $i_{SD}$  and  $i_{SL}$  resulting from the dark current and the photocurrent, respectively.

$$i_n = \sqrt{i_j^2 + i_{SD}^2 + i_{SL}^2} \text{ [A]} \quad \dots\dots (2)$$

If a reverse voltage is not applied as in Figure 1-4, then  $i_j$  is given by equation (3).

$$i_j = \sqrt{\frac{4kTB}{R_{sh}}} \text{ [A]} \quad \dots\dots (3)$$

k: Boltzmann's constant  
T: absolute temperature of element  
B: noise bandwidth

When a reverse voltage is applied as in Figure 1-7, then there is always a dark current and the  $i_{SD}$  is as shown in equation (4).

$$i_{SD} = \sqrt{2q I_D B} \text{ [A]} \quad \dots\dots (4)$$

q: electron charge  
 $I_D$ : dark current

If photocurrent ( $I_L$ ) is generated by incident light and  $I_L \gg 0.026/R_{sh}$  or  $I_L \gg I_D$ , then the shot noise current resulting from the photocurrent is a predominant source of noise current expressed by equation (5).

$$i_n \approx i_{SL} = \sqrt{2q I_L B} \text{ [A]} \quad \dots\dots (5)$$

The amplitude of these noise sources are each proportional to the square root of noise bandwidth (B) and so are expressed

in units of  $A/Hz^{1/2}$  normalized by B.

The lower limit of light detection for photodiodes is usually expressed as the incident light level required to generate a current equal to the noise current as expressed in equation (3) or (4), which is termed the noise equivalent power (NEP).

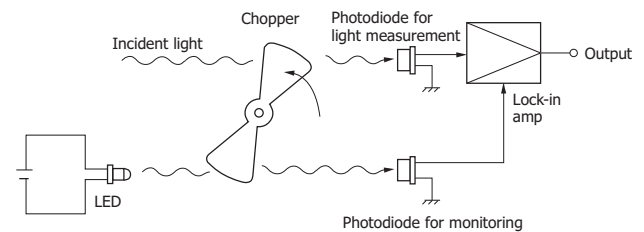
$$NEP = \frac{i_n}{S} \text{ [W/Hz}^{1/2}] \quad \dots\dots (6)$$

$i_n$ : noise current  
S: photosensitivity

In the circuit shown in Figure 1-7 (b), noise from the op amp and  $R_f$  must be taken into account along with the photodiode noise described above. Moreover, in high-frequency regions the transfer function including capacitive components such as photodiode capacitance ( $C_t$ ) and feedback capacitance ( $C_f$ ) must also be considered. The lower limit of light detection will be larger than the NEP defined in equation (6) because there are effects from the amplifier's temperature drift and flicker noise in low-frequency regions, gain peaking described later on, and others.

In the case of InGaAs PIN photodiodes, cooled types are often used to improve the lower limit of light detection. Periodically turning the incident light on and off by some means and synchronously detecting only signals of the same frequency are also effective in removing noise from unwanted bands. This allows the detection limit to approach the NEP [Figure 1-8].

[Figure 1-8] Synchronous measurement method



KPDC0007EB

### □ Spectral response

InGaAs PIN photodiodes are roughly divided into the following three types according to their spectral response ranges.

- ① Standard type:  
sensitive in a spectral range from 0.9 to 1.7  $\mu m$
- ② Short-wavelength enhanced type:  
variant of the standard type and having extended sensitivity to shorter wavelengths
- ③ Long wavelength type:  
sensitive in a spectral range extending to longer wavelengths than standard type

The cutoff wavelength ( $\lambda_c$ ) on the long wavelength side of photodiodes is expressed by equation (7) using their band gap energy ( $E_g$ ).

$$\lambda_c = \frac{1.24}{E_g} [\mu\text{m}] \dots\dots (7)$$

Eg: band gap energy [eV]

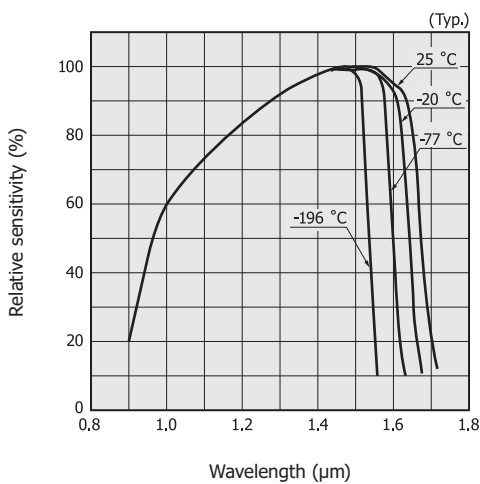
The InGaAs light absorption layer in the standard type and short-wavelength enhanced type has a band gap energy of 0.73 eV. In the long wavelength type, this band gap energy is reduced by changing the ratio of elements making up the InGaAs light absorption layer in order to extend the cutoff wavelength to the longer wavelength side.

InGaAs PIN photodiodes are fabricated with a semiconductor layer called the cap layer which is formed on the InGaAs light absorption layer to suppress the surface leakage current that can cause noise. Light at wavelengths shorter than the cutoff wavelength of the semiconductor comprising the cap layer is almost totally absorbed by the cap layer and so does not reach the light absorption layer, and therefore does not contribute to sensitivity. In the short-wavelength enhanced type, this cap layer is thinned to less than 1/10th the cap layer thickness for the standard type by improving the wafer structure and wafer process. This reduces the amount of light absorbed by the cap layer and so increases the amount of light reaching the light absorption layer, improving the sensitivity at short wavelengths.

Because the band gap energy increases as the element temperature is lowered, the spectral response range of InGaAs PIN photodiodes shifts to the shorter wavelength side as the element temperature decreases. This also reduces the amount of noise, so D\* (detectivity) increases [Figure 1-10]. The spectral transmittance of the window materials used in the InGaAs/GaAs PIN photodiodes is shown in Figure 1-11.

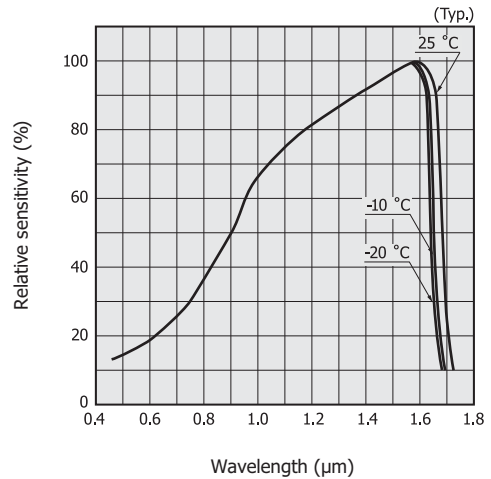
[Figure 1-9] Spectral response

(a) InGaAs PIN photodiode (standard type)



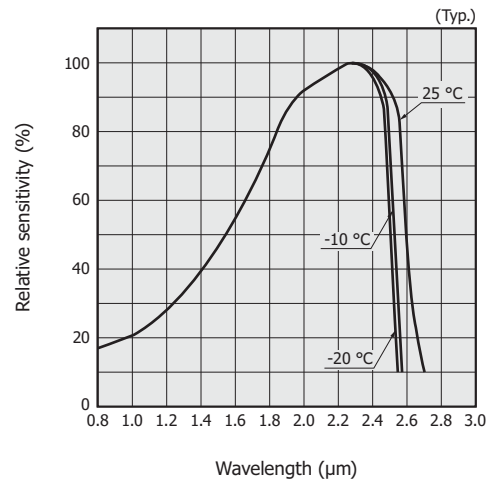
KIRDB0132EA

(b) InGaAs PIN photodiode (short-wavelength enhanced type)



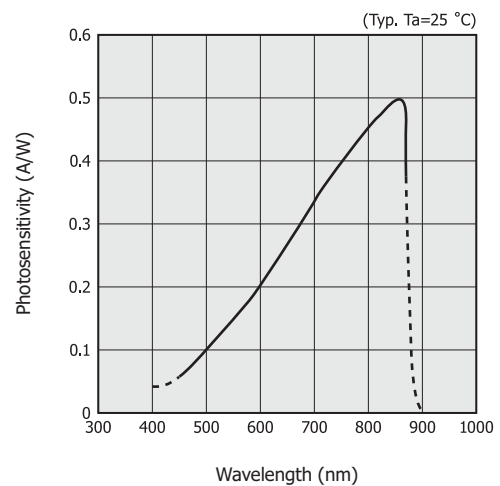
KIRDB0395EA

(c) InGaAs PIN photodiode [long wavelength type (up to 2.6 μm)]



KIRDB0133EC

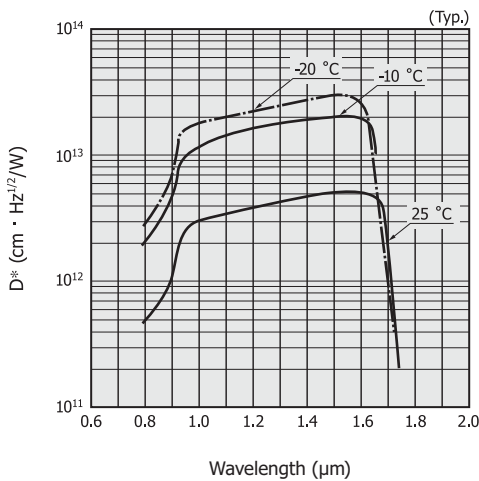
(d) GaAs PIN photodiode



KGPD80044EA

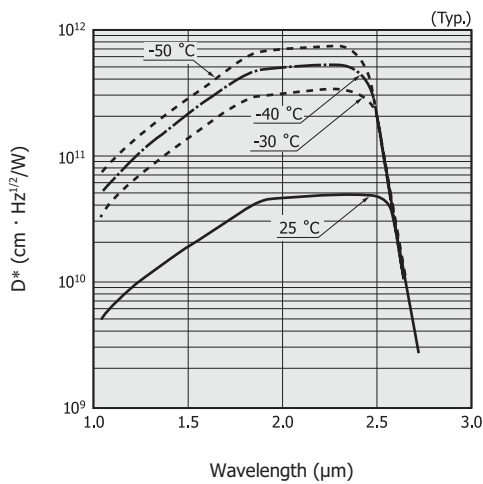
[Figure 1-10]  $D^*$  vs. wavelength (InGaAs PIN photodiode)

(a) Standard type



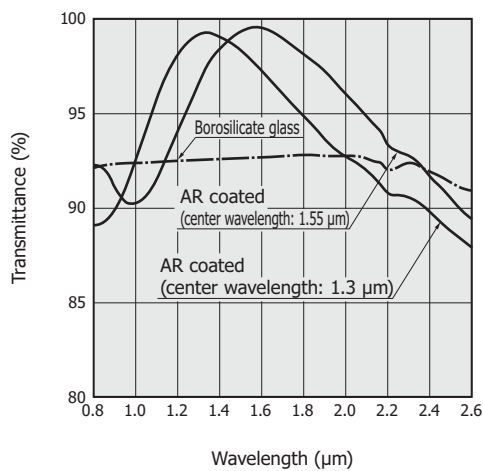
KIRDB0134EA

(b) Long wavelength type (up to 2.6 μm)



KIRDB0135EA

[Figure 1-11] Spectral transmittance of window materials (typical example)



KIRDB0550EA

**Time response characteristics**

The time response is a measure of how fast the generated carriers are extracted to an external circuit as output current, and is generally expressed as the rise time or

cutoff frequency.

The rise time ( $t_r$ ) is the time required for the output signal to rise from 10% to 90% of its peak value and is expressed by equation (8).

$$t_r = 2.2C_t(R_L + R_s) \dots\dots (8)$$

$C_t$ : terminal capacitance  
 $R_L$ : load resistance  
 $R_s$ : series resistance

Generally,  $R_s$  can be disregarded because  $R_L \gg R_s$ . To make the rise time smaller, the  $C_t$  and  $R_L$  should be lowered, but  $R_L$  is determined by an external factor and so cannot freely be changed.  $C_t$  is proportional to the photosensitive area ( $A$ ) and is inversely proportional to the square root of the reverse voltage ( $V_R$ ).

$$C_t \propto \frac{A}{\sqrt{V_R}} \dots\dots (9)$$

Higher response speeds can be obtained by applying a reverse voltage to a photodiode with a small photosensitive area.

Charges generated by light absorbed outside the PN junction sometimes take several microseconds or more to diffuse and reach the electrode. When the time constant of  $C_t \times R_L$  is small, this diffusion time determines response speeds. In applications requiring fast response, be careful not to allow light to strike outside the photosensitive area.

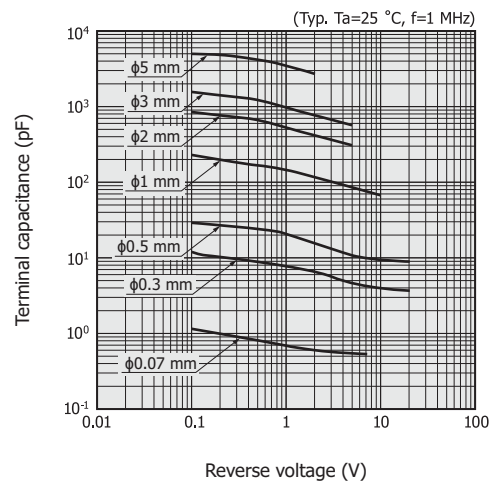
The approximate relationship between the rise time  $t_r$  (unit: s) and cutoff frequency  $f_c$  (unit: Hz) is expressed by equation (10).

$$t_r = \frac{0.35}{f_c} \dots\dots (10)$$

For details on time response, see “1-8 Response speed” in section 1, “Si Photodiodes,” in chapter 2, “Si photodiodes.”

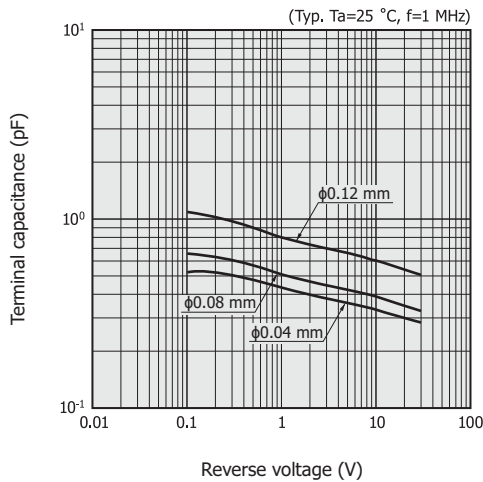
[Figure 1-12] Terminal capacitance vs. reverse voltage

(a) InGaAs PIN photodiodes (standard type)



KIRDB0331EC

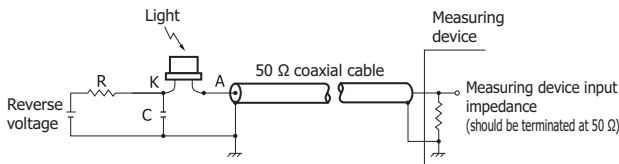
**(b) GaAs PIN photodiodes**



KGPD80059EA

Figure 1-13 shows a high-speed light detection circuit using an InGaAs PIN photodiode. This is a specific example of a connection based on the circuit shown in Figure 1-7 (a) and uses a 50 Ω load resistance. The series resistance R and ceramic capacitor C reduce the noise from the reverse voltage power supply and also reduce the power supply impedance seen from the photodiode. The resistance R also functions to protect the photodiode, and its value should be selected so that the voltage drop caused by the maximum photocurrent will be sufficiently smaller than the reverse voltage. The photodiode and capacitor leads, coaxial cable wires, and the like carrying high-speed pulses should be kept as short as possible.

**[Figure 1-13] High-speed light detection circuit (InGaAs PIN photodiode)**



KPDC0009EA

**Temperature characteristics**

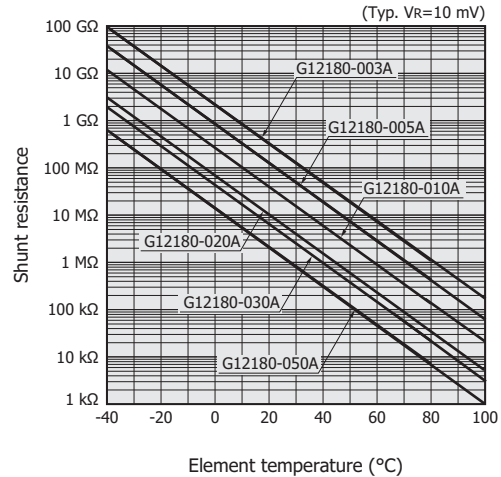
As described in “Spectral response” in section 1-1, “Characteristics,” the spectral response changes with the element temperature. Figure 1-14 shows temperature characteristics of shunt resistance of InGaAs PIN photodiodes. Here, decreasing the element temperature reduces the dark current and increases the shunt resistance and thereby improves the S/N.

The dark current increases exponentially as the element temperature rises. The relationship between the dark current  $I_{Dx}$  of the element temperature  $x$  and the dark current  $I_{Dy}$  of the element temperature  $y$  is given by equation (11). The dark current temperature coefficient “a” varies depending on the band gap energy of the detector. It also varies depending on the reverse voltage applied to the detector.

$$I_{Dx} = I_{Dy} \times a^{x-y} \dots\dots\dots (11)$$

Hamamatsu provides one-stage and two-stage TE-cooled InGaAs PIN photodiodes that can be used at a constant operating temperature (or by cooling).

**[Figure 1-14] Shunt resistance vs. element temperature [InGaAs PIN photodiodes (standard type)]**



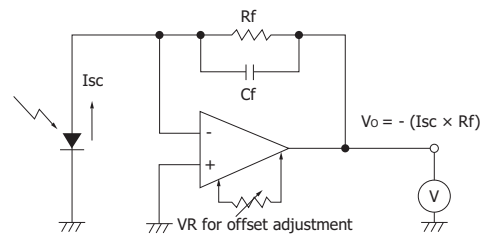
KIRD80544EA

**1 - 2 How to use**

**Connection to an op amp**

A connection example with an op amp is shown in Figure 1-15. The input impedance of the op amp circuit in Figure 1-15 is the value of the feedback resistance  $R_f$  divided by the open-loop gain and so is very small. This yields excellent linearity.

**[Figure 1-15] Connection example**



KIRD0040EB

Precautions when using an op amp are described below.

(1) Selecting feedback resistance

In Figure 1-15, the short circuit current  $I_{sc}$  is converted to the output voltage  $V_o$ , which is  $I_{sc} \times R_f$ . If  $R_f$  is larger than the photodiode shunt resistance  $R_{sh}$ , then the op amp's input noise voltage and input offset voltage are multiplied by  $(1 + R_f/R_{sh})$  and superimposed on the output voltage. The op amp bias current error also increases, so there is a limit to the  $R_f$  increase.

The feedback capacitance  $C_f$  is mainly used to prevent oscillation. A capacitance of several picofarads is sufficient for this purpose.

This feedback circuit has a time constant of  $C_f \times R_f$  and serves as a noise filter. It also limits the response speed at the same time, so the feedback resistance value must be carefully selected to match the application. Error due to an offset voltage can usually be reduced to less than 1 mV by connecting a variable resistor to the offset adjustment terminals on the op amp. For application circuit examples, see “1-10 Application circuit examples,” in section 1, “Si Photodiodes,” in chapter 2, “Si photodiodes.”

## (2) Selecting an op amp

Since the actual input impedance of an op amp is not infinite, some bias current will flow into or out of the input terminals. This might cause an error depending on the amplitude of the detected current.

The bias current which flows in an FET-input op amp is sometimes lower than 0.1 pA. Bipolar op amps, however, have bias currents ranging from several hundred picoamperes to several hundred nanoamperes.

In general, the bias current of FET-input op amps doubles for every 10 °C increase in temperature, while the bias current of bipolar op amps decreases. Because of this, bipolar type op amps also need to be considered when designing circuits for high temperature applications. Just as with offset voltages, the error voltage due to a bias current can be fine-tuned by connecting a variable resistor to the offset adjustment terminals of the op amp.

## 2. InGaAs APD

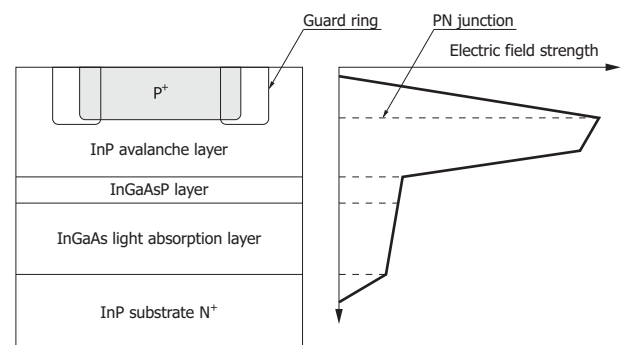
InGaAs APDs (avalanche photodiodes) are infrared detectors having an internal multiplication function. When an appropriate reverse voltage is applied, they multiply photocurrent to achieve high sensitivity and high-speed response.

InGaAs APDs are sensitive to light in the 1 μm band where optical fibers exhibit low loss, and so are widely used for optical fiber communications. Light in the 1 μm band is highly safe for human eyes (eye-safe) and is also utilized for FSO (free space optics) and optical distance measurement.

### 2-1 Operating principle

When electron-hole pairs are generated in the depletion layer of an APD with a reverse voltage applied to the PN junction, the electric field created across the PN junction causes the electrons to drift toward the N<sup>+</sup> side and the holes to drift toward the P<sup>+</sup> side. The drift speed of these carriers depends on the electric field strength. However, when the electric field is increased, the carriers are more likely to collide with the crystal lattice so that the drift speed becomes saturated at a certain speed. If the reverse voltage is increased even further, some carriers that escaped collision with the crystal lattice will have a great deal of energy. When these carriers collide with the crystal lattice, ionization takes place in which electron-hole pairs are newly generated. These electron-hole pairs then create additional electron-hole pairs in a process just like a chain reaction. This is a phenomenon known as avalanche multiplication. APDs are photodiodes having an internal multiplication function that utilizes this avalanche multiplication.

[Figure 2-1] Structure and electric field profile (InGaAs APD)



KIRD0077EA

Because the band gap energy of InGaAs is small, applying a high reverse voltage increases the dark current. To cope with this, InGaAs APDs employ a structure in which the InGaAs light absorption layer that generates electron-hole pairs by absorbing light is isolated from the InP avalanche layer that multiplies carriers generated by light utilizing avalanche multiplication. APDs with this structure for separating the light absorption layer

from the avalanche layer are called the SAM (separated absorption and multiplication) type. Hamamatsu InGaAs APDs employ this SAM type.

## 2-2 Characteristics

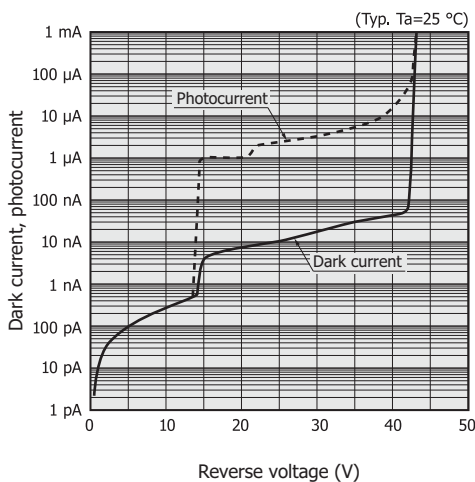
### Dark current vs. reverse voltage characteristics

APD dark current  $I_D$  consists of two dark current components:  $I_{DS}$  (surface leakage current and the like flowing through the interface between the PN junction and the surface passivation film) which is not multiplied, and  $I_{DG}$  (recombination current, tunnel current, and diffusion current generated inside the semiconductor, specified at  $M=1$ ) which is multiplied.

$$I_D = I_{DS} + M \cdot I_{DG} \dots\dots (1)$$

Figure 2-2 shows an example of current vs. reverse voltage characteristics for an InGaAs APD. Since the InGaAs APD has the structure shown in Figure 2-1, there is no sensitivity unless the depletion layer extends to the InGaAs light absorption layer at a low reverse voltage.

[Figure 2-2] Dark current and photocurrent vs. reverse voltage (G8931-04)



KAPDB0123EA

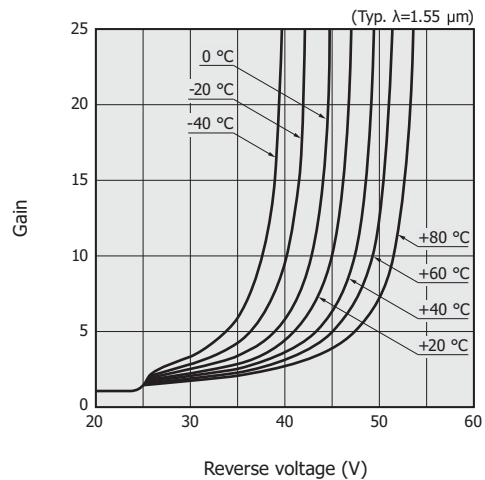
In our InGaAs APDs, under the condition that they are not irradiated with light, the reverse voltage that causes a reverse current of 100  $\mu\text{A}$  to flow is defined as the breakdown voltage ( $V_{BR}$ ), and the reverse current at a reverse voltage  $V_R = 0.9 \times V_{BR}$  is defined as the dark current.

### Gain vs. reverse voltage characteristics

InGaAs APD gain characteristics depend on the electric field strength applied to the InP avalanche layer, so the gain usually increases as the reverse voltage is increased. But increasing the reverse voltage also increases the dark current, and the electric field applied to the InP avalanche layer decreases due to a voltage drop in the

series resistance component of the photodiode. This means that the gain will not increase even if the reverse voltage is increased higher than that level. If the APD is operated at or near the maximum gain, the voltage drop in the serial resistance component will become large, causing a phenomenon in which photocurrent is not proportional to the incident light level.

[Figure 2-3] Temperature characteristics of gain (G8931-04)

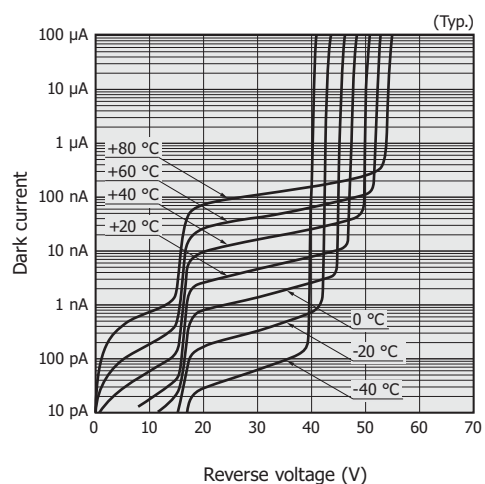


KIRDB0396EA

InGaAs APD gain varies with temperature as shown in Figure 2-3. The gain at a certain reverse voltage becomes smaller as the temperature rises. This phenomenon occurs because the crystal lattice vibrates more heavily as the temperature rises, increasing the possibility that the carriers accelerated by the electric field may collide with the lattice before reaching an energy level sufficient to cause ionization. To obtain a constant output, the reverse voltage must be adjusted to match changes in temperature or the element temperature must be kept constant.

Figure 2-4 is a graph showing the temperature dependence of dark current vs. reverse voltage characteristics in the range from -40 to +80  $^{\circ}\text{C}$ .

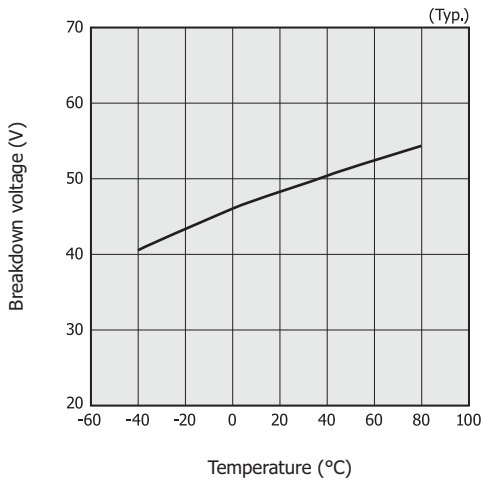
[Figure 2-4] Temperature characteristics of dark current (G8931-04)



KIRDB0397EA

Temperature characteristic of breakdown voltage is shown in Figure 2-5.

[Figure 2-5] Breakdown voltage vs. temperature (G8931-04)



KIRDB0398EA

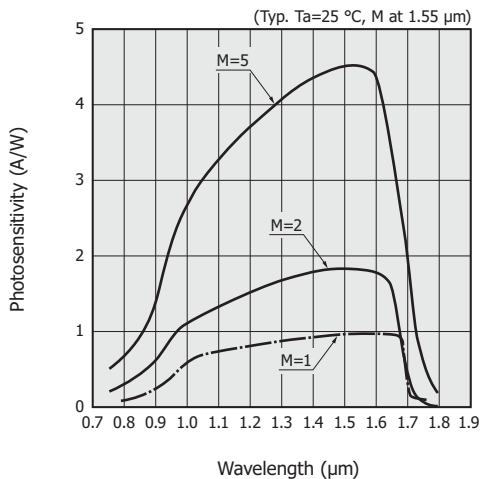
### Spectral response

When light with energy higher than the band gap energy of the semiconductor is absorbed by the photodiode, electron-hole pairs are generated and detected as signals. The following relationship exists between the band gap energy  $E_g$  (unit: eV) and the cutoff wavelength  $\lambda_c$  (unit:  $\mu\text{m}$ ), as shown in equation (2).

$$\lambda_c = \frac{1.24}{E_g} [\mu\text{m}] \quad \dots\dots (2)$$

As light absorption material, InGaAs APDs utilize InGaAs whose composition is lattice-matched to InP. The band gap energy of that material is 0.73 eV at room temperature. The InGaAs APD cutoff wavelength is therefore approx. 1.7  $\mu\text{m}$ . The InGaAs APD spectral response differs depending on the gain [Figure 2-6]. Sensitivity on the shorter wavelength side decreases because short-wavelength light is absorbed by the InP avalanche layer.

[Figure 2-6] Spectral response (G8931-20)



KIRDB0120EB

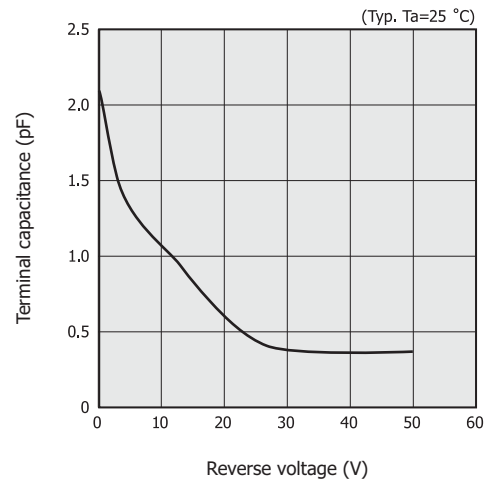
Temperature characteristics of the InGaAs band gap energy affect temperature characteristics of InGaAs APD spectral response. As the temperature rises, the InGaAs band gap energy becomes smaller, making the cutoff wavelength longer.

InGaAs APDs have an anti-reflection film formed on the light incident surfaces in order to prevent the quantum efficiency from deteriorating by reflection on the APD.

### Terminal capacitance vs. reverse voltage characteristics

The graph curve of terminal capacitance vs. reverse voltage characteristics for InGaAs APDs differs from that of InGaAs PIN photodiodes [Figure 2-7]. This is because their PN junction positions are different.

[Figure 2-7] Terminal capacitance vs. reverse voltage (G8931-04)



KIRDB0124EB

### Noise characteristics

In InGaAs APDs, the gain for each carrier has statistical fluctuations. Multiplication noise known as excess noise is therefore added during the multiplication process. The InGaAs APD shot noise ( $I_n$ ) becomes larger than the InGaAs PIN photodiode shot noise, and is expressed by equation (3).

$$I_n^2 = 2q (I_L + I_{DG}) B M^2 F + 2q I_{DS} B \quad \dots\dots (3)$$

- q : electron charge
- $I_L$  : photocurrent at M=1
- $I_{DG}$  : dark current component multiplied
- $I_{DS}$  : dark current component not multiplied
- B : bandwidth
- M : gain
- F : excess noise factor

The number of electron-hole pairs generated during the time that a carrier moves a unit distance in the semiconductor is referred to as the ionization rate. The ionization rate of electrons is defined as " $\alpha$ " [ $\text{cm}^{-1}$ ] and that of holes as " $\beta$ " [ $\text{cm}^{-1}$ ]. These ionization rates are important parameters that determine the multiplication mechanism. The ratio of  $\beta$  to  $\alpha$  is called the ionization rate ratio (k), which is a parameter that indicates the InGaAs APD noise.

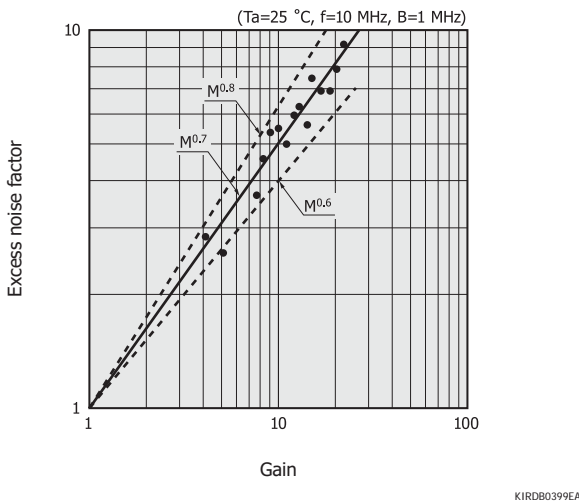
$$k = \frac{\beta}{\alpha} \dots\dots\dots (4)$$

The ionization rate ratio is a physical constant inherent to individual semiconductor materials. The ionization rate ratio (k) for InP is greater than 1 since the hole ionization rate is larger than the electron ionization rate. Therefore, in InGaAs APDs, the holes of the electron-hole pairs generated by light absorption in the InGaAs layer will drift toward the InP avalanche layer due to the reverse voltage. The excess noise factor (F) is expressed using the ionization rate ratio (k) as in equation (5).

$$F = M k + \left(2 - \frac{1}{M}\right) (1 - k) \dots\dots\dots (5)$$

The excess noise factor can also be approximated as  $F=M^x$  (where x is the excess noise index). Figure 2-8 shows an example of the relationship between the InGaAs APD excess noise factor and the gain. In this figure, the excess noise index is approximately 0.7.

[Figure 2-8] Excess noise factor vs. gain (G8931-04, typical example)



As already explained, InGaAs APDs generate noise accompanying the multiplication process, so excess noise increases as the gain becomes higher. The output signal also increases as the gain becomes higher, so the S/N is maximized at a certain gain. The S/N for an InGaAs APD can be expressed by equation (6).

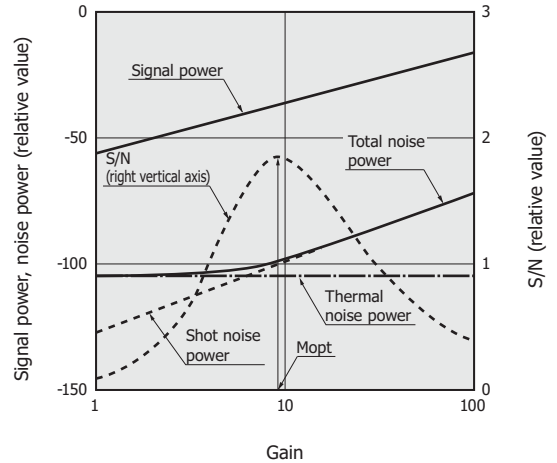
$$S/N = \frac{I_L^2 M^2}{2q (I_L + I_{DG}) B M^2 F + 2q I_{DS} B + \frac{4k T B}{R_L}} \dots\dots (6)$$

- 2q (I<sub>L</sub> + I<sub>DG</sub>) B M<sup>2</sup> F: excess noise
- 2q I<sub>DS</sub> B: shot noise
- k : Boltzmann's constant
- T : absolute temperature
- R<sub>L</sub>: load resistance

The optimal gain (M<sub>opt</sub>) can be found from conditions that maximize the value of equation (6), and given by equation (7) if I<sub>DS</sub> is ignored.

$$M_{opt} = \left[ \frac{4k T}{q (I_L + I_{DG}) \cdot x \cdot R_L} \right]^{\frac{1}{2+x}} \dots\dots\dots (7)$$

[Figure 2-9] Signal power and noise power vs. gain



**Time response characteristics**

Major factors that determine the response speed of an APD are the CR time constant, drift time (time required for the carrier to traverse the depletion layer), and the multiplication time. The cutoff frequency determined by the CR time constant is given by equation (8).

$$f_c(CR) = \frac{1}{2\pi C_t R_L} \dots\dots\dots (8)$$

- C<sub>t</sub>: terminal capacitance
- R<sub>L</sub>: load resistance

To increase the cutoff frequency determined by the CR time constant, the terminal capacitance should be reduced. This means that a smaller photosensitive area with a thicker depletion layer is advantageous for raising the cutoff frequency. The relationship between cutoff frequency (f<sub>c</sub>) and the rise time (tr) is expressed by equation (9).

$$tr = \frac{0.35}{f_c(CR)} \dots\dots\dots (9)$$

The drift time cannot be ignored if the depletion layer is made thick. The drift time tr<sub>d</sub> and cutoff frequency f<sub>c</sub>(tr<sub>d</sub>) determined by the drift time are expressed by equations (10) and (11), respectively.

$$tr_d = \frac{W}{v_{ds}} \dots\dots\dots (10)$$

$$f_c(tr_d) = \frac{0.44}{tr_d} \dots\dots\dots (11)$$

- W : thickness of depletion layer
- v<sub>ds</sub>: drift speed

The hole drift speed in InGaAs becomes saturated at an electric field strength of approx. 10<sup>4</sup> V/cm, and the drift speed at that point is approx. 5 × 10<sup>6</sup> cm/s. A thinner depletion layer is advantageous in improving the cutoff frequency f<sub>c</sub>(tr<sub>d</sub>) determined by the drift time, so the cutoff frequency f<sub>c</sub>(tr<sub>d</sub>) determined by the drift time has a trade-off relation with the cutoff frequency f<sub>c</sub>(CR)

determined by the CR time constant.

The carriers passing through the avalanche layer repeatedly collide with the crystal lattice, so a longer time is required to move a unit distance than the time required to move in areas outside the avalanche layer. The time (multiplication time) required for the carriers to pass through the avalanche layer becomes longer as the gain increases.

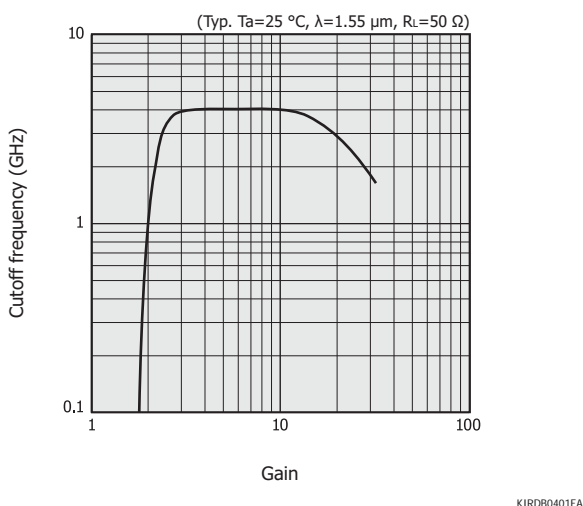
In general, at a gain of 5 to 10, the CR time constant and drift time are the predominant factors in determining the response speed, and at a gain higher than 10, the multiplication time will be the predominant factor.

One cause that degrades the response speed in a low gain region is a time delay due to the diffusion current of carriers from outside the depletion layer. This time delay is sometimes as large as a few microseconds and appears more prominently in cases where the depletion layer has not extended enough versus the penetration depth of incident light into the InGaAs. To achieve high-speed response, it is necessary to apply a reverse voltage higher than a certain level, so that the InGaAs light absorption layer becomes fully depleted. If the InGaAs light absorption layer is not fully depleted, the carriers generated by light absorbed outside the depletion layer might cause “trailing” that degrades the response characteristics.

When the incident light level is high and the resulting photocurrent is large, the attraction force of electrons and holes in the depletion layer serves to cancel out the electric field, so the carrier drift speed in the InGaAs light absorption layer becomes slower and time response is impaired. This phenomenon is called the space charge effect and tends to occur especially when the optical signal is interrupted.

The relationship between the InGaAs APD cutoff frequency and gain is shown in Figure 2-10.

[Figure 2-10] Cutoff frequency vs. gain (G8931-04)

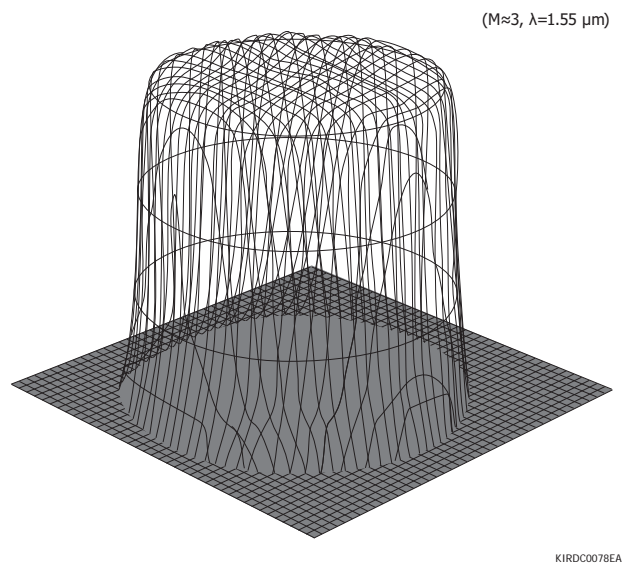


### □ Sensitivity uniformity of photosensitive area

Since a large reverse voltage is applied to InGaAs APDs to apply a high electric field across the PN junction, this electric field might concentrate locally especially at or near the junction and tend to cause breakdowns. To prevent this, Hamamatsu InGaAs APDs use a structure having a guard

ring formed around the PN junction. This ensures uniform sensitivity in the photosensitive area since the electric field is applied uniformly over the entire photosensitive area.

[Figure 2-11] Sensitivity distribution in photosensitive area (G8931-20)



## 2 - 3 How to use

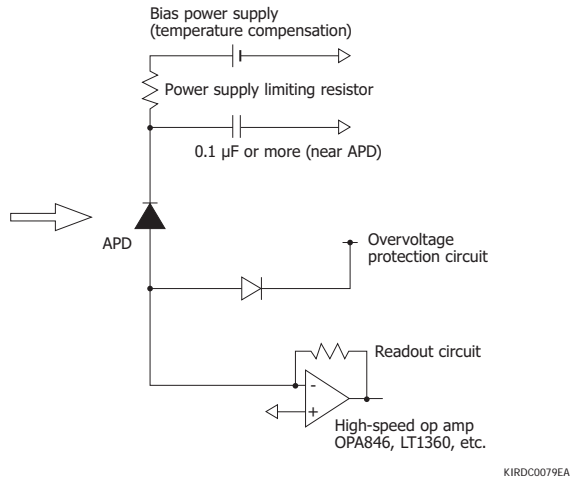
InGaAs APDs can be handled nearly the same as InGaAs PIN photodiodes and Si APDs. However, the following precautions should be taken.

- ① The maximum reverse current for InGaAs APDs is 2 mA. So there is a need to add a protective resistor and then install a current limiting circuit to the bias circuit.
- ② A low-noise readout circuit may damage the first stage in response to excess voltage. To prevent this, a protective circuit should be connected to divert any excess input voltage to the power supply voltage line.
- ③ APD gain changes with temperature. To use an APD over a wide temperature range, the reverse voltage must be controlled to match the temperature changes or the APD temperature must be maintained at a constant level.
- ④ When detecting low-level light signals, the lower detection limit is determined by the shot noise. If background light enters the APD, then the S/N might deteriorate due to shot noise from background light. In this case, effects from the background light must be minimized by using optical filters, improving laser modulation, and/or restricting the angle of view. Because of their structure, the excess noise index for InGaAs APDs is especially large compared to Si APD, so effects from shot noise including excess noise must be taken into account.

A connection example is shown in Figure 2-12.

We welcome requests for customization of InGaAs APD modules.

[Figure 2-12] Connection example



## 3. ROSA modules

Here we introduce a ROSA (receiver optical sub-assembly) module with a built-in InGaAs PIN photodiode designed to meet the demand for high-speed, miniaturized optical communication modules.

### 3-1 Structure

ROSA has a housing with a mating part for an optical fiber connector, and a TO-CAN type metal-package photosensor is fitted into the housing. Housings are available in metal and plastic types. The metal type shown in Figure 3-1 has an internal low-reflection structure that suppresses the optical return loss with 27 dB min. The plastic type shown in Figure 3-2 has a molded structure formed with an aspherical lens. It has high optical return loss with 12 dB min. and so is used for short-distance communications.

[Figure 3-1] Structure of metal type ROSA

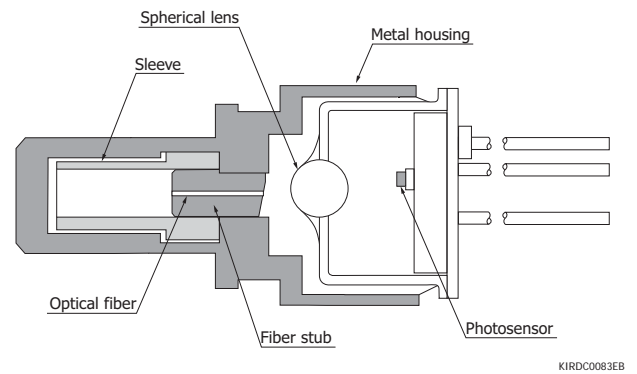
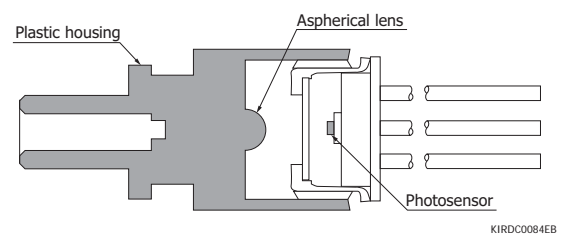


[Figure 3-2] Structure of plastic type ROSA



### 3-2 Features

#### (1) SONET/SDH

SONET/SDH is mainly utilized in trunk lines using long-wavelength single-mode fibers. SONET/SDH standards are grouped as shown in Table 3-1.

Since SONET/SDH requires high sensitivity and low optical return loss, a metal type ROSA with a low-reflection structure is used [Figure 3-1].

Transmissions over long distances greater than 80 km require even higher sensitivity, so APDs should be used instead of PIN photodiodes.

## (2) Ethernet

Ethernet standards are grouped according to optical fiber and transmission distance as shown in Table 3-2.

OMA (optical modulation amplitude) is a measurement parameter for determining optical transmitter characteristics. OMA is expressed by equation (1).

$$\text{OMA} = 2 \times \text{Pave} \times (1 - \text{ER}) / (1 + \text{ER}) \dots\dots (1)$$

Pave: average power  
ER : extinction ratio

When using long-wavelength single-mode fibers for long-distance transmission, low optical return loss is required so a metal type ROSA is employed the same as for SONET/SDH. A plastic type ROSA can be used if high optical return loss is not a problem.

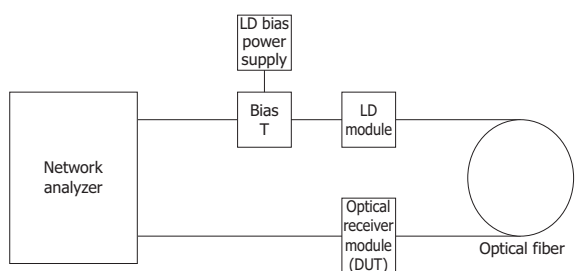
For short-distance transmissions within 300 m, multimode fibers with large core diameters and a short-wavelength near 850 nm are used.

## 3-3 Characteristics

### Frequency response

Figure 3-3 shows a setup for measuring frequency characteristics of an optical receiver module. The laser diode (LD) should have a sufficiently wide bandwidth compared to the optical receiver module (DUT: device under test), and the measurement system should be calibrated using an LD whose frequency characteristics are already known, so that effects from the measurement system's frequency characteristics can be ignored.

[Figure 3-3] Setup for frequency characteristic measurement (optical receiver module)



KIRDC0054EA

[Table 3-1] SONET/SDH standards (data rate: 9.95328 Gbps)

Communication standard	Wavelength (nm)	Dispersion compensation method	Maximum transmission distance (km)	Maximum sensitivity (dBm)	Minimum sensitivity (dBm)	Maximum optical return loss (dB)	Minimum allowable extinction ratio (dB)
SR-1	1310	-	7	-1	-11	-14	6
SR-2	1550	-	25	-1	-14	-27	8.2
IR-1	1310	-	20	-1	-11	-14	6
IR-2	1550	-	40	-1	-14	-27	8.2
IR-3	1550	-	40	-1	-13	-27	8.2
LR-1	1310	-	40	-9	-20	-27	6
LR-2	1550	PCH	80	-7	-24	-27	9
LR-2a	1550	PDC	80	-9	-26	-27	10
LR-2b	1550	SPM	80	-3	-14	-27	8.2
LR-2c	1550	PCH	80	-9	-26	-27	10
LR-3	1550	-	80	-3	-13	-27	8.2
VR-2a	1550	PDC	120	-9	-25	-27	10
VR-2b	1550	PDC & SPM	120	-7	-23	-27	8.2
VR-3	1550	-	120	-9	-24	-27	8.2

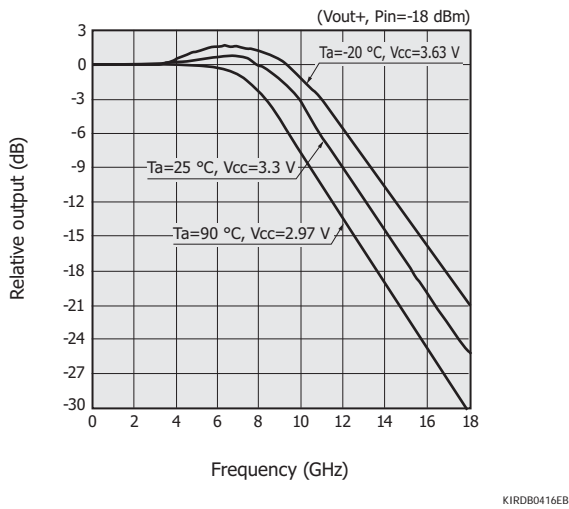
[Table 3-2] Ethernet standards (data rate: 10.3125 Gbps)

Communication standard	Fiber	Wavelength (nm)	Maximum transmission distance	Maximum sensitivity (dBm)	Minimum sensitivity (dBm)	Minimum sensitivity OMA (dBm)	Maximum optical return loss (dB)	Minimum allowable extinction ratio (dB)
SR	MMF	850	300 m	-1	-9.9	-11.1	-12	3
LR	SMF	1310	10 km	0.5	-14.4	-12.6	-12	3.5
ER	SMF	1550	40 km	-1	-15.8	-14.1	-26	3

Optical receiver modules used for digital optical communications usually contain an internal AGC (automatic gain control) amplifier or a limiting amplifier to obtain a wide dynamic range. In frequency characteristic measurement, if an AGC amplifier is used, the LD power is adjusted to a level that turns off the AGC, and if a limiting amplifier is used, the LD power is adjusted to a level that is within the linear range.

Figure 3-4 shows the frequency characteristics and their temperature characteristics of a 10 Gbps PIN ROSA. The cutoff frequency ( $f_c$ ) is defined as the frequency at which the gain drops by 3 dB from the value at low frequencies.

[Figure 3-4] Frequency characteristics (10 Gbps PIN ROSA, typical example)

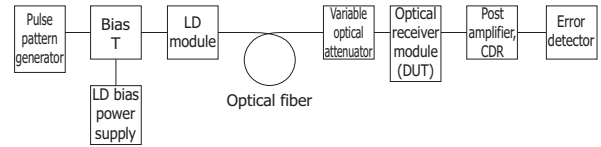


### Bit error rate

Figure 3-5 shows a setup for measuring the bit error rate. A pulse pattern generator outputs a pseudo-random pattern that modulates the LD. The power level of this modulated light is changed by a variable optical attenuator and is input to the optical receiver module (DUT). The

output from the optical receiver module (DUT) is input to the error detector via the post amplifier and CDR (clock data recovery), and then the bit error rate is measured by comparing the received pattern with the pattern driving the LD.

[Figure 3-5] Setup for measuring bit error rate



The minimum light input power which can maintain a specified bit error rate is called the minimum sensitivity. The maximum light input power is called the maximum sensitivity (overload).

Figure 3-6 shows typical examples of bit error rates in a plastic type 10 Gbps PIN ROSA.

[Figure 3-6] Bit error rate (plastic type 10 Gbps PIN ROSA, typical example)

#### (a) Minimum sensitivity

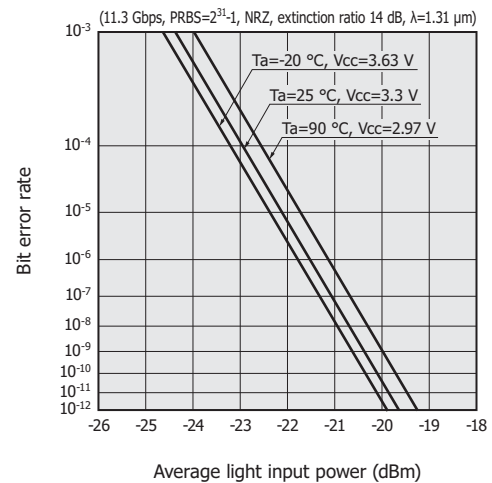


[Table 3-3] Electrical and optical characteristics (plastic type 10 Gbps PIN ROSA: G12072-54)

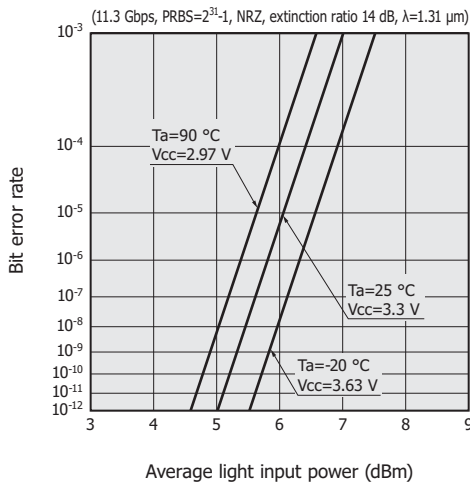
Parameter	Symbol	Condition	Min.	Typ.	Max.	Unit
Photosensitivity*1	R	$\lambda=1.31 \mu\text{m}$ , $\text{Pin}=-10 \text{ dBm}$	0.7	0.8	-	A/W
Supply current	$I_{\text{CC}}$	Dark state, $R_L=\infty$	-	28	50	mA
Cutoff frequency	$f_c$	$\lambda=1.31 \mu\text{m}$ , $-3 \text{ dB}$ , $\text{Pin}=-18 \text{ dBm}$ , $f_{\text{ref}}=1 \text{ GHz}$	7	10	-	GHz
Low cutoff frequency	$f_{c-L}$	$\lambda=1.31 \mu\text{m}$ , $-3 \text{ dB}$ , $\text{Pin}=-18 \text{ dBm}$ , $f_{\text{ref}}=100 \text{ MHz}$ , extinction ratio=6 dB	-	30	100	kHz
Transimpedance*2	$T_z$	$f=1 \text{ GHz}$ , $\text{Pin}=-18 \text{ dBm}$	1.0	2.25	-	k $\Omega$
Minimum sensitivity (average)	$P_{\text{min}}$	11.3 Gbps, $\lambda=1.31 \mu\text{m}$ , PRBS=2 <sup>31</sup> -1, BER=10 <sup>-12</sup> , Extinction ratio=14 dB	-	-19.5	-17.5	dBm
Maximum sensitivity (average)	$P_{\text{max}}$		+2	+5	-	
Output amplitude	$V_{\text{omax}}$	Differential, $\text{Pin}=-5 \text{ dBm}$	200	280	400	mVp-p
RSSI offset current	$I_{\text{RSSI}}$	Dark state, $R_L=\infty$ , $V_{\text{CC}}=3.3 \text{ V}$	2.5	10	17	$\mu\text{A}$
Optical return loss*3	ORL	$\lambda=1.31 \mu\text{m}$	12	14	-	dB

\*1: Photosensitivity =  $2 \times (\text{RSSI output current} - \text{RSSI offset current}) / \text{Incident light level}$

\*2: Single-ended (Vout+) measurement

\*3: Low-reflection metal type (ORL  $\geq 27 \text{ dB}$ ) is also available.

(b) Maximum sensitivity



KIRD0419EB

3 - 4 Precautions

Precautions during handling

Opto-semiconductors are easily damaged or destroyed by static charges, surges from power supplies and test equipment, and leakage current from soldering irons, etc. So the following precautions must be taken when handling these devices.

- Wear a grounding wrist strap during soldering, assembly, measurement, and so on, and if necessary use an ionizer to suppress generation of static electricity.
- Make sure that the device, workbench, jigs, soldering iron tip, and measuring instruments are all at the same voltage potential.
- Be careful about possible surges from the power supply when turning it on, and apply Vpd first and then Vcc (this order may vary depending on the product).
- The excess stress should not be given to optical receiver module housing during assembly or operation to avoid deterioration of optical coupling efficiency.
- Dirt or scratches on the fiber end faces of the optical receiver module make it difficult for signal light to enter the photodiode and cause an apparent drop in sensitivity. Check carefully for dirt or scratches on the fiber end faces and clean them if dirt is found.

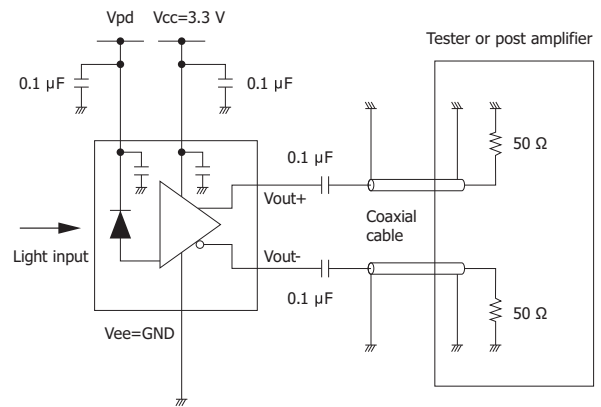
Precautions during mounting

Take the following precautions during mounting in order to bring out the full performance of the high-speed device. Figure 3-7 shows a measurement circuit example for an optical receiver module.

- During the mounting, keep the leads as short as possible and solder them to the board.
- Connect a capacitor with good frequency characteristics as a bypass capacitor between power supply line and ground, in the shortest possible distance.

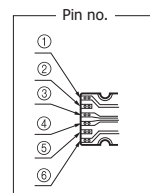
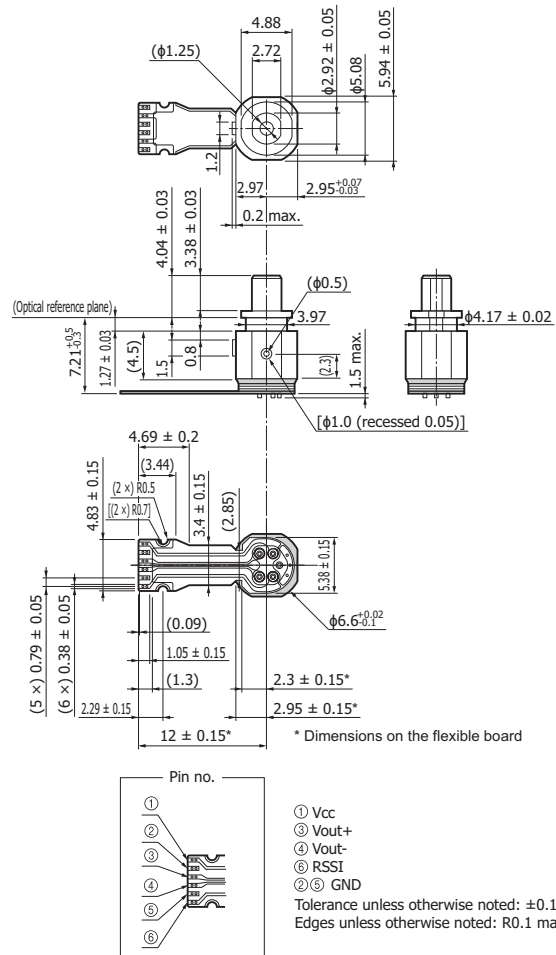
- The leads may sometimes break or weaken due to mechanical stress, so take care during mounting. Hamamatsu provides a ROSA with a flexible cable that reduces the mechanical stress applied to the lead when connected to the circuit board [Figure 3-8].
- Caution is also needed with boards where receiver modules are mounted. Figure 3-9 shows an evaluation board example. One side is used for the signal lines and ground pattern, and the reverse side serves as a ground pattern. The ground patterns on both sides are connected by through-holes. The signal line pattern is a coplanar line or microstrip line whose impedance matches that of the latter-stage circuit.

[Figure 3-7] Measurement circuit example for optical receiver module



KIRD0053EA

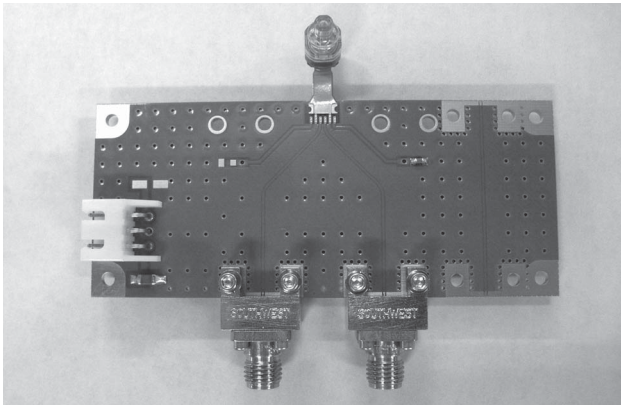
[Figure 3-8] Dimensional outline (G12072-54, unit: mm)



- ① Vcc
  - ② Vout+
  - ③ Vout-
  - ④ RSSI
  - ⑤ GND
  - ⑥ GND
- Tolerance unless otherwise noted:  $\pm 0.1$   
Edges unless otherwise noted: R0.1 max.

KIRDA0214EA

[Figure 3-9] Evaluation board for 10 Gbps PIN ROSA



Note: If a module requires capacitive coupling, then switch the measuring instrument to AC coupling, or insert a coupling capacitor or DC block between the measuring instrument and the evaluation board.

As shown in Figure 3-10, a coplanar line has a structure containing a transmission line conductor and a ground conductor in the same plane on one side of the dielectric substrate. The characteristic impedance is determined by the dielectric constant of the substrate, the width of the transmission line conductor, and the gap between the transmission line conductor and ground conductor.

A microstrip line as shown in Figure 3-11 has a structure containing a transmission line conductor on one side of the dielectric substrate, and a ground conductor on the backside of that substrate. The characteristic impedance is determined by the dielectric constant and thickness of the substrate, and by the width of the transmission line conductor.

[Figure 3-10] Coplanar line

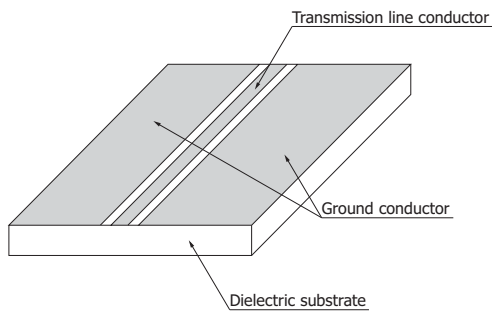
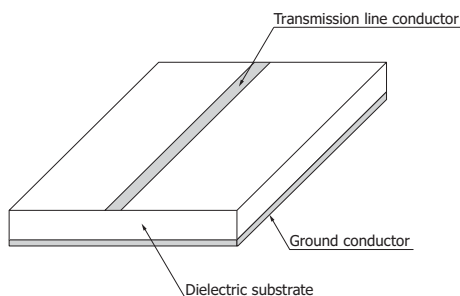


[Figure 3-11] Microstrip line



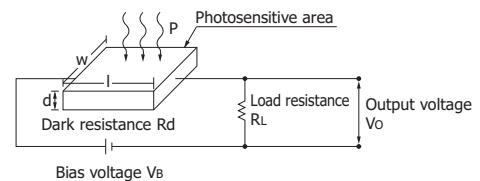
## 4. PbS/PbSe photoconductive detectors

PbS and PbSe photoconductive detectors are infrared detectors utilizing a photoconductive effect that lowers the electrical resistance when illuminated with infrared light. Compared to other detectors used in the same wavelength regions, PbS and PbSe photoconductive detectors offer the advantages of higher detection capability and operation at room temperature. However, the dark resistance, sensitivity, and response speeds change according to the ambient temperature, so caution is required.

### 4 - 1 Operating principle

When infrared light enters a PbS/PbSe photoconductive detector, the number of carriers increases, causing its resistance to lower. A circuit like that shown in Figure 4-1 is used to extract the signal as a voltage, and photosensitivity is expressed in units of V/W.

[Figure 4-1] Output signal measurement circuit for photoconductive detector



The output voltage ( $V_o$ ) is expressed by equation (1).

$$V_o = \frac{R_L}{R_d + R_L} \cdot V_B \dots\dots\dots (1)$$

The change ( $\Delta V_o$ ) in  $V_o$ , which occurs due to a change ( $\Delta R_d$ ) in the dark resistance ( $R_d$ ) when light enters the detector, is expressed by equation (2).

$$\Delta V_o = - \frac{R_L V_B}{(R_d + R_L)^2} \cdot \Delta R_d \dots\dots\dots (2)$$

$\Delta R_d$  is then given by equation (3).

$$\Delta R_d = - R_d \frac{q (\mu_e + \mu_h)}{\sigma} \cdot \frac{\eta \tau \lambda P A}{l w d h c} \dots\dots\dots (3)$$

- q : electron charge
- $\mu_e$ : electron mobility
- $\mu_h$ : hole mobility
- $\sigma$  : electric conductivity
- $\eta$  : quantum efficiency
- $\tau$  : carrier lifetime
- $\lambda$  : wavelength
- P : incident light level [W/cm<sup>2</sup>]
- A : photosensitive area [cm<sup>2</sup>]
- h : Planck's constant
- c : Speed of light in vacuum

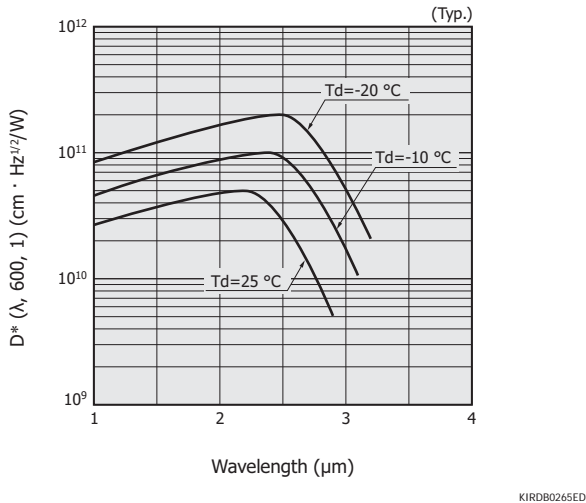
## 4 - 2 Characteristics

### Spectral response

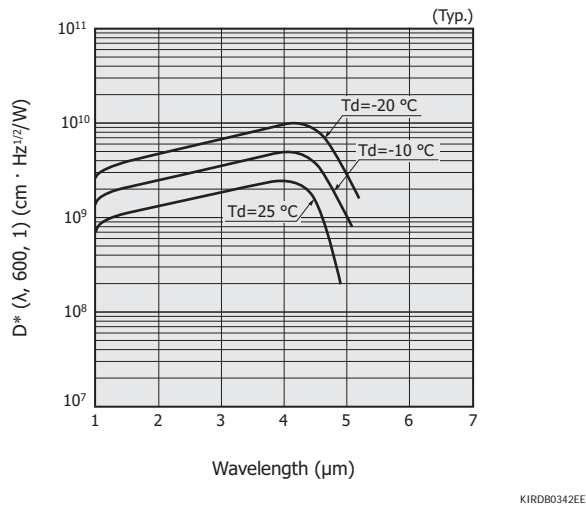
Temperature characteristics of PbS/PbSe band gap energy have a negative coefficient, so cooling the detector shifts its spectral response range to the long wavelength side.

[Figure 4-2] Spectral response

#### (a) PbS photoconductive detector (P9217 series)



#### (b) PbSe photoconductive detector (P9696 series)



### Time response characteristics

Sensitivity frequency characteristic of PbS/PbSe photoconductive detectors (when a chopper is used) is given by equation (4).

$$R(f) = \frac{R(0)}{\sqrt{1 + 4\pi^2 f^2 \tau^2}} \dots\dots (4)$$

- R(f) : frequency response
- R(0) : response at zero frequency
- f : chopping frequency
- τ : time constant

Because PbS/PbSe photoconductive detector noise has a typical 1/f noise spectrum, D\* is expressed by equation (5).

$$D^*(f) = \frac{k\sqrt{f}}{\sqrt{1 + 4\pi^2 f^2 \tau^2}} [\text{cm}\cdot\text{Hz}^{1/2}/\text{W}] \dots\dots (5)$$

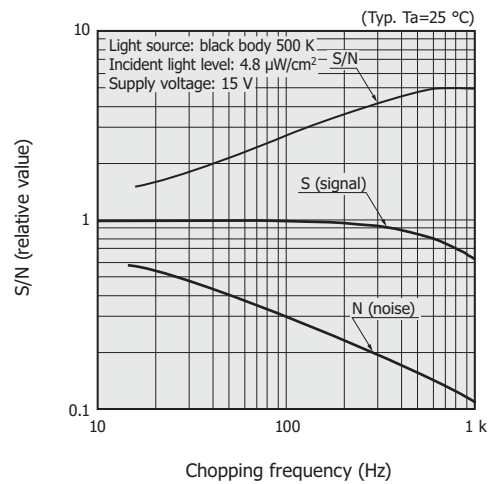
D\*(f) is maximized at  $f = \frac{1}{2\pi\tau}$ .

S/N frequency characteristics of PbS/PbSe photoconductive detectors are shown in Figure 4-3.

Sensitivity frequency characteristics of PbS photoconductive detectors at a room temperature (+25 °C) and at a TE-cooled temperature (-20 °C) are shown in Figure 4-4.

[Figure 4-3] S/N vs. chopping frequency

#### (a) PbS photoconductive detector



#### (b) PbSe photoconductive detector

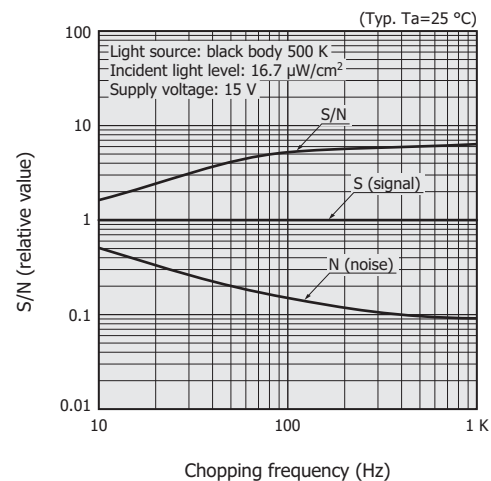
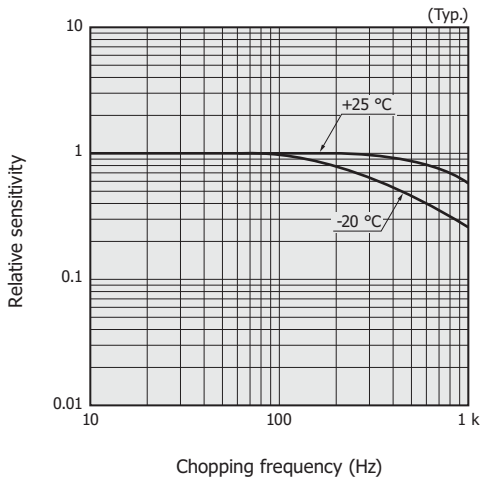


[Figure 4-4] Sensitivity vs. chopping frequency (PbS photoconductive detector)



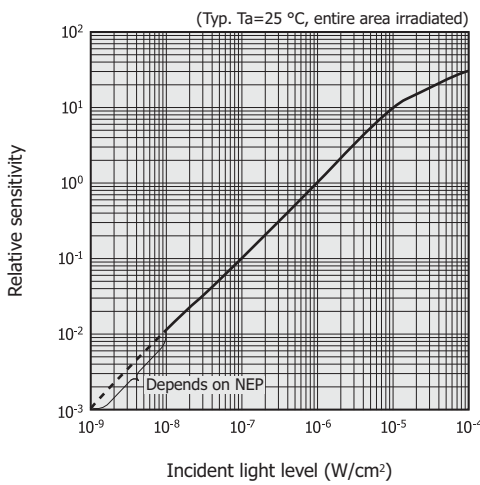
KIRDB0083EC

### Linearity

Figure 4-5 shows the relationship between incident light level and detector output. The lower linearity limits of PbS/PbSe photoconductive detectors are determined by their NEP.

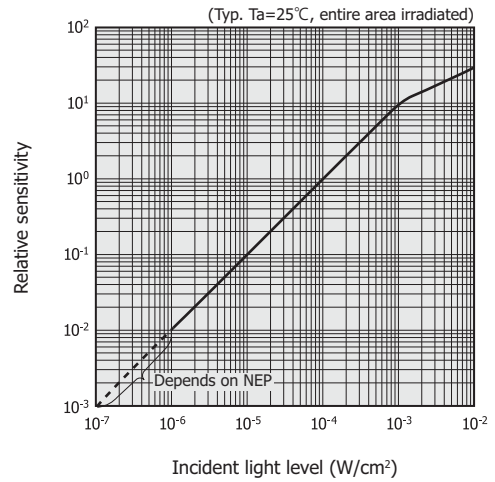
[Figure 4-5] Linearity

#### (a) PbS photoconductive detector



KIRDB0050EA

#### (b) PbSe photoconductive detector



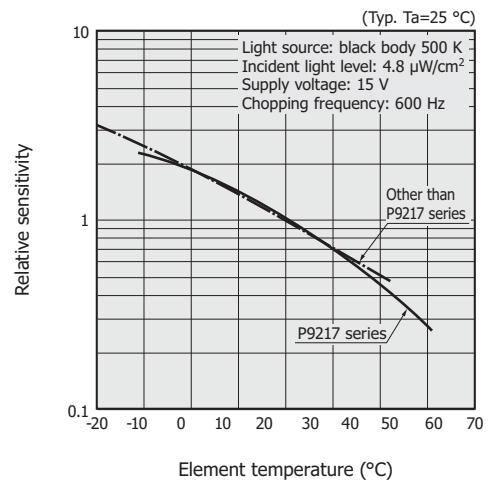
KIRDB0056EA

### Temperature characteristics

Photosensitivity, dark resistance, and rise time of PbS/PbSe photoconductive detectors vary as the element temperature changes [Figures 4-6 and 4-7].

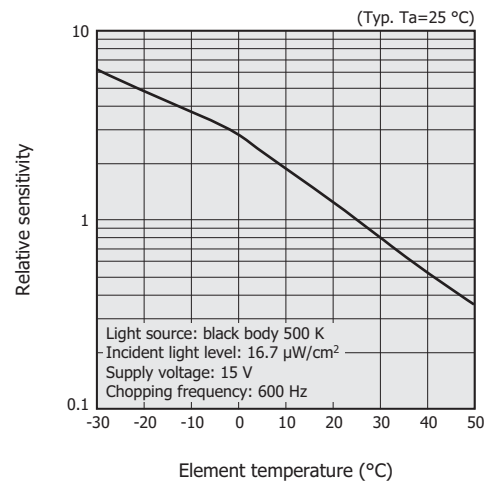
[Figure 4-6] Photosensitivity vs. element temperature

#### (a) PbS photoconductive detector



KIRDB0048ED

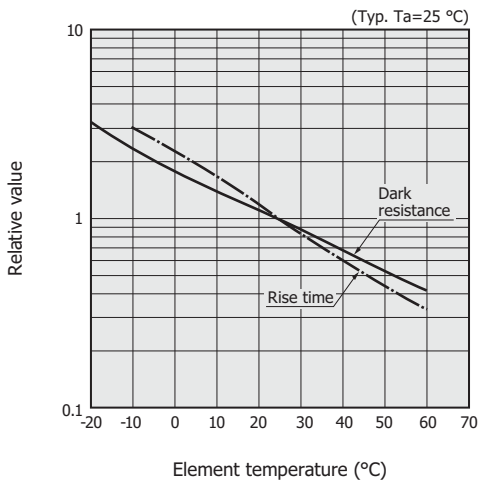
#### (b) PbSe photoconductive detector



KIRDB0042EC

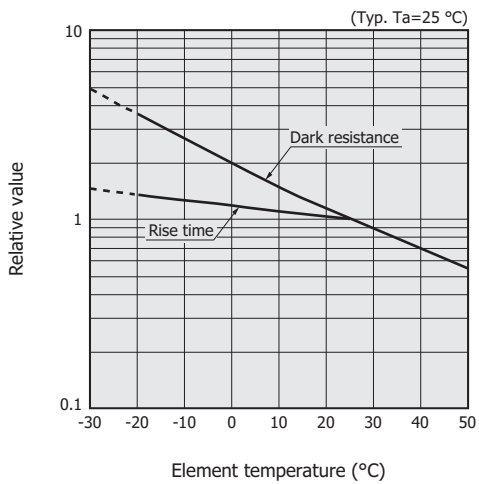
[Figure 4-7] Dark resistance and rise time vs. element temperature

(a) PbS photoconductive detector (P9217 series)



KIRDB0303EA

(b) PbSe photoconductive detector

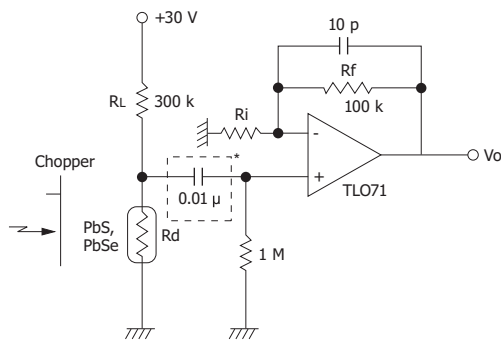


KIRDB0443EC

### 4 - 3 How to use

To operate PbS/PbSe photoconductive detectors, a chopper is usually used to acquire AC signals like the circuit shown in Figure 4-8.

[Figure 4-8] Connection example



\* Not necessary when acquiring DC signals

KIRDC0012EC

The signal voltage ( $V_o$ ) in Figure 4-8 is expressed by equation (6).

$$V_o = -i_s \times R_d \left(1 + \frac{R_f}{R_i}\right) \dots\dots\dots (6)$$

$i_s$ : signal current

#### Temperature compensation

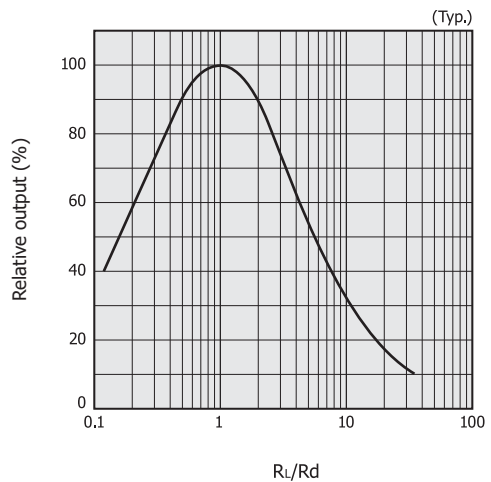
Since the sensitivity and dark resistance of PbS/PbSe photoconductive detectors drift according to the element temperature, some measures must be taken to control the temperature.

The TE-cooled PbS/PbSe photoconductive detectors contain a thermistor intended to maintain the element temperature at a constant level and to suppress the temperature-dependent drift. In some cases, the detectors are kept warm at a constant temperature by a heater or the like. However, this may not only reduce sensitivity but also speed up deterioration in the detector so use caution.

#### Load resistance

The largest signal can be obtained when the load resistance ( $R_L$ ) and dark resistance ( $R_d$ ) are the same value. The relationship between the output signal and  $R_L/R_d$  is shown in Figure 4-9.

[Figure 4-9] Output vs.  $R_L/R_d$



KIRDB0137EA

#### Chopping frequency

As stated in “Time response characteristics” in section 4-2, “Characteristics,” the  $D^*$  is maximized at  $f = \frac{1}{2\pi\tau}$ . Narrowing the amplifier bandwidth will reduce the noise and improve the S/N. In low-light level measurement, the chopping frequency and bandwidth must be taken into account.

#### Voltage dependence

The noise of PbS/PbSe photoconductive detectors suddenly increases when the voltage applied to the detector exceeds a certain value. Though the signal increases in proportion to the voltage, the detector should be used at as low a voltage

as possible within the maximum supply voltage listed in our datasheets.

**Photosensitive area**

To obtain a better S/N, using a small-area PbS/PbSe photoconductive detector and narrowing the incident light on the detector to increase the light level per unit area on the detector prove more effective than using a large-area detector. If the incident light deviates from the photosensitive area or light other than signal light strikes the detector, this may lower the S/N, so use extra caution to avoid these problems.

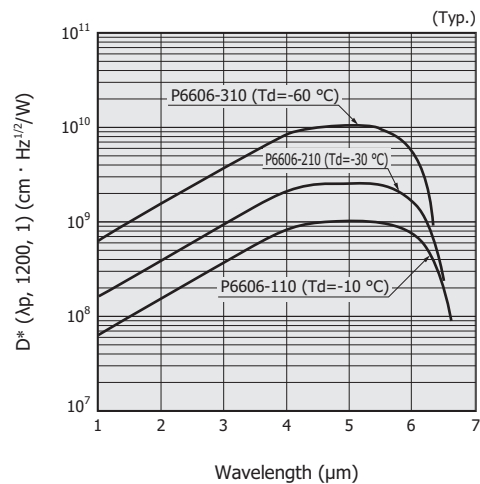
**Precautions for use (PbS photoconductive detectors)**

Characteristics of PbS photoconductive detectors may change if stored at high temperatures or under visible light (room illumination), ultraviolet light, etc. Always store these detectors in a cool, dark place. If these detectors are used under visible light or the like, then provide light-shielding to block that light.

## 5. InSb photoconductive detectors

InSb photoconductive detectors are infrared detectors capable of detecting light up to approx. 6.5  $\mu\text{m}$ . InSb photoconductive detectors are easy to handle since they are thermoelectrically cooled (liquid nitrogen not required).

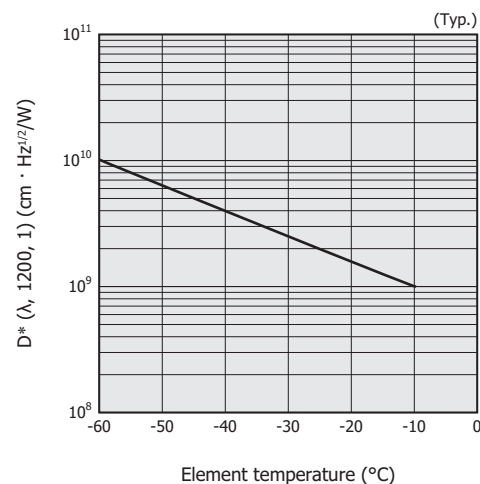
[Figure 5-1] Spectral response



KIRDB0166ED

The band gap energy in InSb photoconductive detectors has a positive temperature coefficient, so cooling the detector shifts its cutoff wavelength to the short-wavelength side. This is the same for InSb photovoltaic detectors.

[Figure 5-2]  $D^*$  vs. element temperature (P6606-310)



KIRDB0167EA

## 6. InAs/InAsSb/InSb photovoltaic detectors

As with InGaAs PIN photodiodes, InAs/InAsSb/InSb photovoltaic detectors are infrared detectors having a PN junction. InAs photovoltaic detectors are sensitive around 3  $\mu\text{m}$ , the same as PbS photoconductive detectors, while InAsSb/InSb photovoltaic detectors are sensitive to the 3 to 5  $\mu\text{m}$  band, the same as PbSe photoconductive detectors.

InAs/InAsSb/InSb photovoltaic detectors offer fast response and a high S/N and so are used in applications different from those for PbS/PbSe photoconductive detectors. We have made an 8  $\mu\text{m}$ -band type available by controlling the composition of the InAsSb photovoltaic detector (a 10  $\mu\text{m}$ -band type is currently in development).

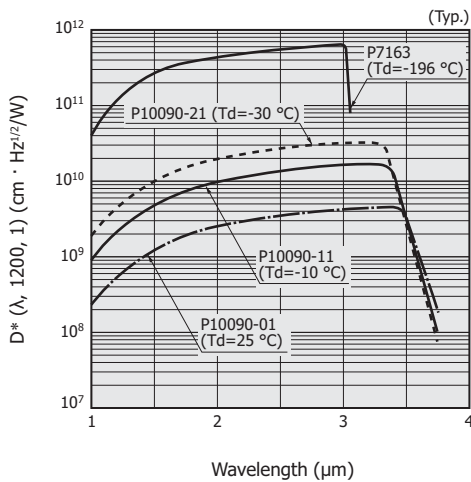
### 6-1 Characteristics

#### Spectral response

InAs photovoltaic detectors include a non-cooled type, TE-cooled type ( $T_d = -10^\circ\text{C}$ ,  $-30^\circ\text{C}$ ), and liquid nitrogen cooled type ( $T_d = -196^\circ\text{C}$ ) which are used for different applications. InAsSb photovoltaic detectors include a TE-cooled type ( $T_d = -30^\circ\text{C}$ ), and liquid nitrogen cooled type ( $T_d = -196^\circ\text{C}$ ). InSb photovoltaic detectors are only available as liquid nitrogen cooled types. Figure 6-1 shows spectral responses of InAs/InAsSb/InSb photovoltaic detectors.

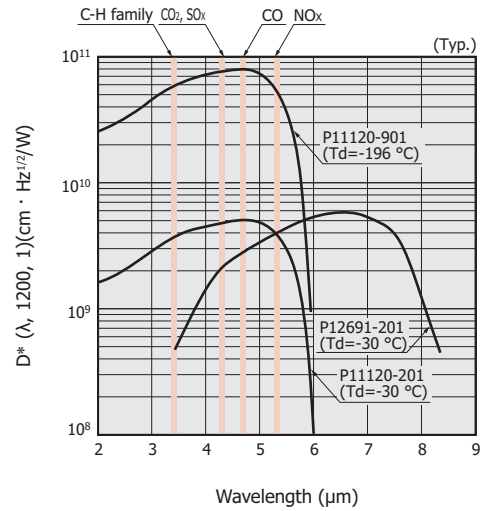
[Figure 6-1] Spectral response

#### (a) InAs photovoltaic detectors



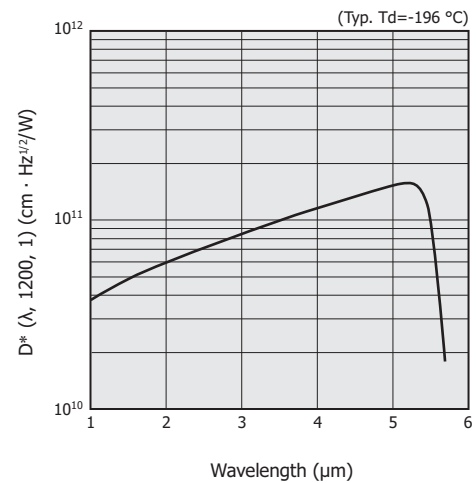
KIRDB0356ED

#### (b) InAsSb photovoltaic detectors



KIRDB0430EE

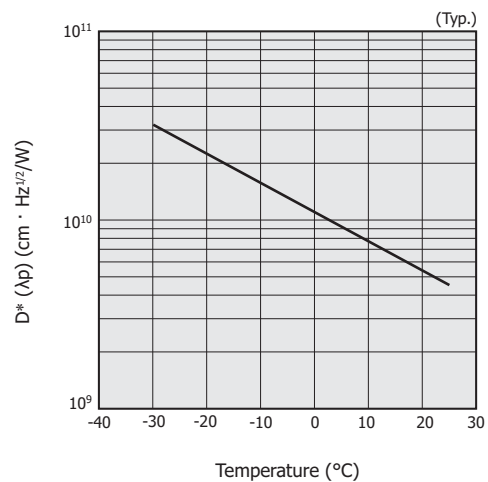
#### (c) InSb photovoltaic detector



KIRDB0063EF

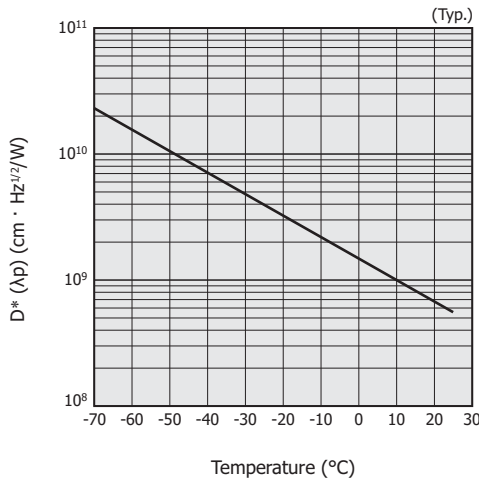
[Figure 6-2]  $D^*$  vs. element temperature

#### (a) InAs photovoltaic detector



KIRDB0555EA

(b) InAsSb photovoltaic detector (P11120-201)



KIRDB0556EA

**Noise characteristics**

InAs/InAsSb/InSb photovoltaic detector noise (i) results from Johnson noise (ij) and shot noise (isd) due to dark current (including photocurrent generated by background light). Each type of noise is expressed by the following equations:

$$i = \sqrt{ij^2 + isd^2} \dots\dots\dots (1)$$

$$ij = \sqrt{4k T B/Rsh} \dots\dots\dots (2)$$

$$isd = \sqrt{2q Id B} \dots\dots\dots (3)$$

- k : Boltzmann's constant
- T : absolute temperature of element
- B : noise bandwidth
- Rsh: shunt resistance
- q : electron charge
- Id : dark current

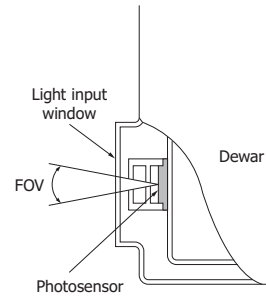
When considering the spectral response range of InSb photovoltaic detectors, background light fluctuations (background radiation noise) from the surrounding areas cannot be ignored. The D\* of InSb photovoltaic detectors is given by equation (4) assuming that the background radiation noise is the only noise source.

$$D^* = \frac{\lambda \sqrt{\eta}}{h c \sqrt{2Q}} [\text{cm} \cdot \text{Hz}^{1/2}/\text{W}] \dots\dots\dots (4)$$

- λ : wavelength
- η : quantum efficiency
- h : Planck's constant
- c : speed of light
- Q : background photon flux [photons/cm<sup>2</sup>·s]

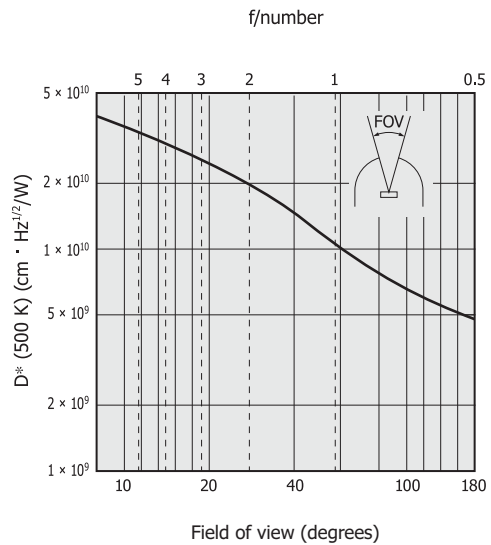
To reduce background radiation noise, the detector's field of view (FOV) must be limited by using a cold shield or unwanted wavelengths must be eliminated by using a cooled band-pass filter. Figure 6-4 shows how the D\* relates to the field of view.

[Figure 6-3] Field of view (FOV)



KIRDC0033EB

[Figure 6-4] D\* vs. field of view



KIRDB0138EB

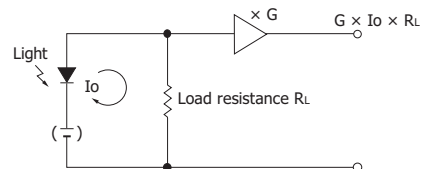
**6 - 2 Precautions**

**Operating circuit**

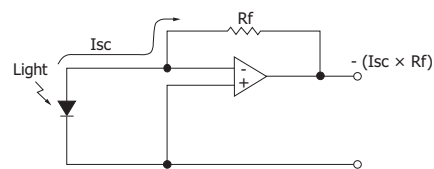
Figure 6-5 shows a connection example for InAs/InAsSb/ InSb photovoltaic detectors. The photocurrent is extracted as a voltage using a load resistor or op amp.

[Figure 6-5] Connection examples (InAs/InAsSb/InSb photovoltaic detector)

(a) When load resistor is connected



(b) When op amp is connected



KPDC0006EC

## Resistance measurement

Measuring the resistance of InAs/InAsSb/InSb photovoltaic detectors with a multimeter might damage the detector. This risk is even higher at room temperature, so always cool the detector when making this measurement.

## Input of visible light (InSb photovoltaic detector)

When visible light or ultraviolet light with energy higher than infrared light enters the InSb photovoltaic detector, an electric charge accumulates on the surface of the element, causing the dark current to increase. The increased dark current also increases noise to degrade the S/N level. Before using, put a cover (such as a double layer of black tape) over the light input window to prevent visible light (room illumination), ultraviolet, or the like from entering the element. Then pour liquid nitrogen into the dewar. If the detector has been exposed to visible light or the like after pouring liquid nitrogen and the dark current has increased, remove the liquid nitrogen from the dewar to return the element temperature back to room temperature. Then redo the above procedure, and the dark current will return to the previous level.

# 7. MCT(HgCdTe) photoconductive detectors

MCT (HgCdTe) photoconductive detectors are infrared detectors whose resistance decreases when illuminated with infrared light. These detectors are mainly used for infrared detection around 5  $\mu\text{m}$  and 10  $\mu\text{m}$ .

## 7 - 1 Characteristics

### Spectral response

The band gap energy of HgCdTe crystal varies according to the composition ratio of HgTe and CdTe. This means that infrared detectors having peak sensitivity at different wavelengths can be fabricated by changing this composition ratio. The relation between band gap energy and cutoff wavelength is shown in equation (1).

$$\lambda_c = \frac{1.24}{E_g} \dots\dots (1)$$

$\lambda_c$ : cutoff wavelength [ $\mu\text{m}$ ]  
 $E_g$ : band gap energy [eV]

Besides the composition ratio, the band gap energy also varies depending on the element temperature.

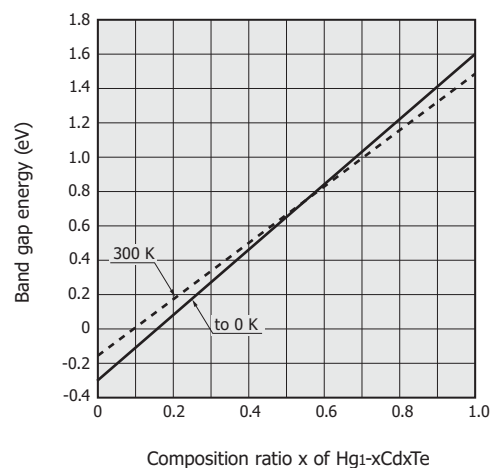
$$E_g = 1.59x - 0.25 + 5.23 \times 10^{-4} T (1 - 2.08x) + 0.327x^3 \dots\dots (2)$$

x: composition ratio of  $\text{Hg}_{1-x}\text{Cd}_x\text{Te}$   
T: absolute temperature

The band gap energy increases as the element temperature rises, causing the peak sensitivity wavelength to shift to the short wavelength side.

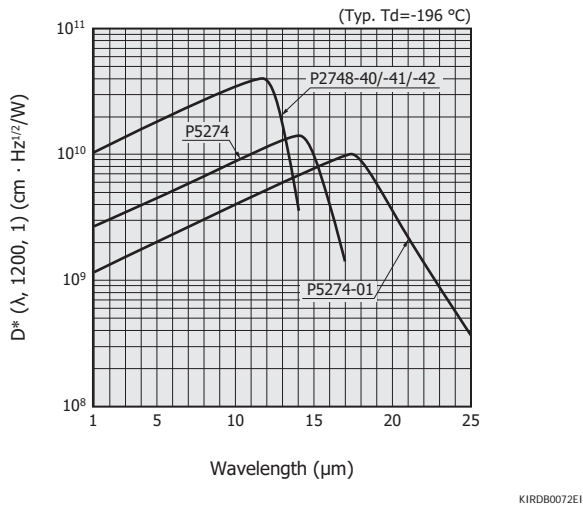
Figure 7-2 shows spectral responses of MCT photoconductive detectors.

[Figure 7-1] Band gap energy vs. composition ratio x of  $\text{Hg}_{1-x}\text{Cd}_x\text{Te}$



KIRD0087EA

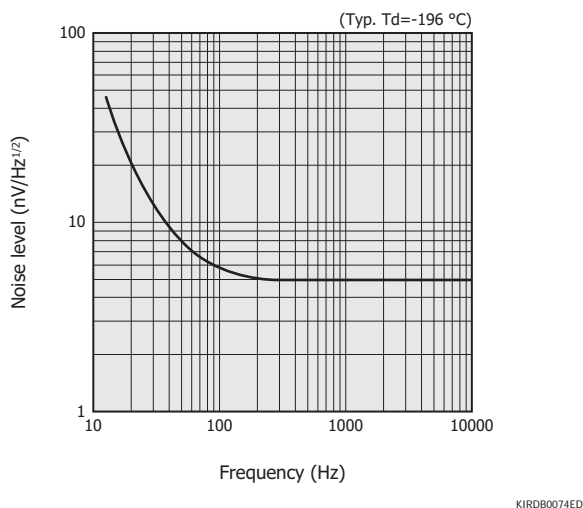
[Figure 7-2] Spectral response (MCT photoconductive detectors)



**□ Noise characteristics**

Noise components in MCT photoconductive detectors include 1/f noise, g-r noise caused by electron-hole recombination, and Johnson noise. The 1/f noise is predominant at low frequencies below several hundred hertz, and the g-r noise is predominant at frequencies higher than that level. Figure 7-3 shows the relationship between the noise level and frequency for an MCT photoconductive detector. In MCT photoconductive detectors with sensitivity at wavelengths longer than 3 μm, fluctuations in background light at 300 K appear as noise and cannot be ignored. But this noise can be reduced by narrowing the field of view.

[Figure 7-3] Noise level vs. frequency (P2748/P5274 series)



**□ Temperature characteristics**

The D\* and spectral response of MCT photoconductive detectors vary according to the element temperature. As the temperature rises, the D\* decreases and the spectral response range shifts to the short-wavelength side. As examples of this, Figures 7-4 and 7-5 show temperature characteristics of D\* and cutoff wavelength, using an

MCT photoconductive detector P2750 for the 3 to 5 μm band.

[Figure 7-4] D\* vs. element temperature (P2750)

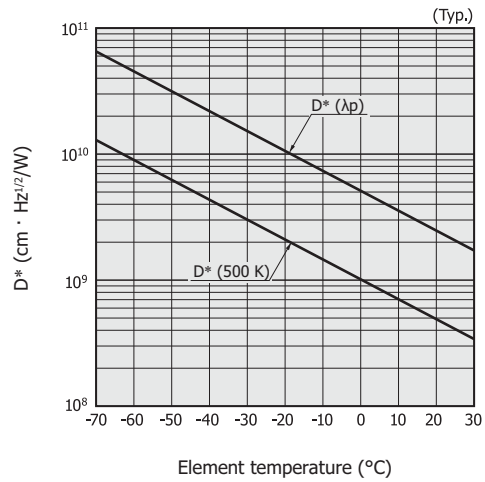
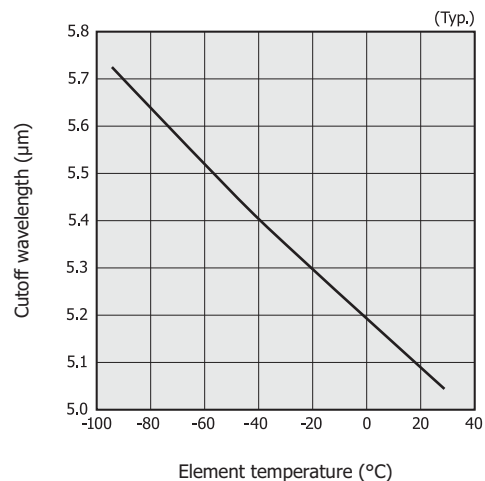
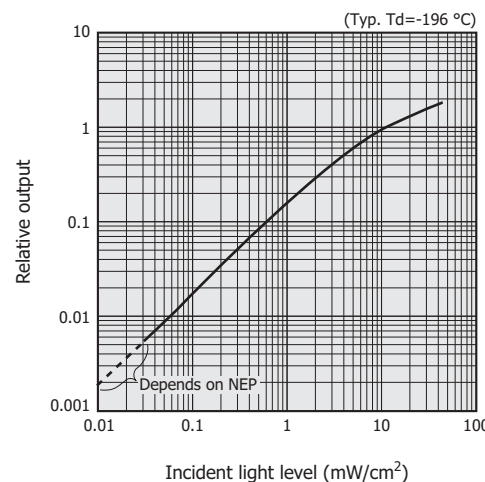


[Figure 7-5] Cutoff wavelength vs. element temperature (P2750)



**□ Linearity**

[Figure 7-6] Linearity (P2748-40)

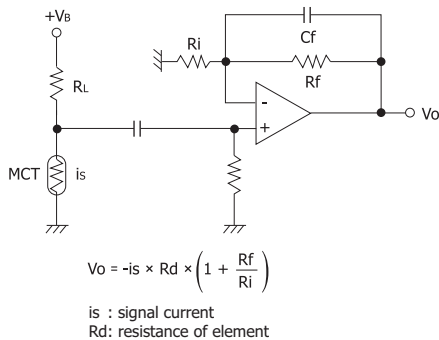


## 7-2 How to use

### Operating circuit

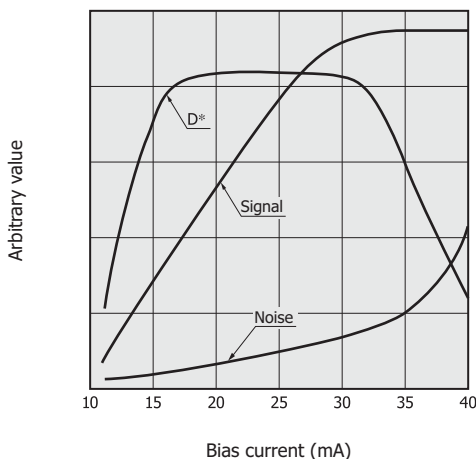
Figure 7-7 shows a connection example for MCT photoconductive detectors. A power supply with low noise and ripple should be used. A load resistance ( $R_L$ ) of several kilohms is generally used to make it a constant current source. As the bias current is raised, both the signal and noise increase [Figure 7-8]. But the noise begins to increase sharply after reaching a particular value, so the bias current should be used in a range where the  $D^*$  becomes constant. Raising the bias current more than necessary increases the element temperature due to Joule heat and degrades the  $D^*$ . This might possibly damage the detector so it should be avoided.

[Figure 7-7] Connection example (MCT photoconductive detector)



KIRD0021EA

[Figure 7-8] Signal, noise, and  $D^*$  vs. bias current (P3257-10, typical example)



KIRDB0091EB

### Ambient temperature

MCT photoconductive detector sensitivity varies with the ambient temperature. As the ambient temperature rises, the background radiation noise increases and the number of carriers in the element also increases. This shortens the average lifetime of the carriers excited by signal light, resulting in lower sensitivity.

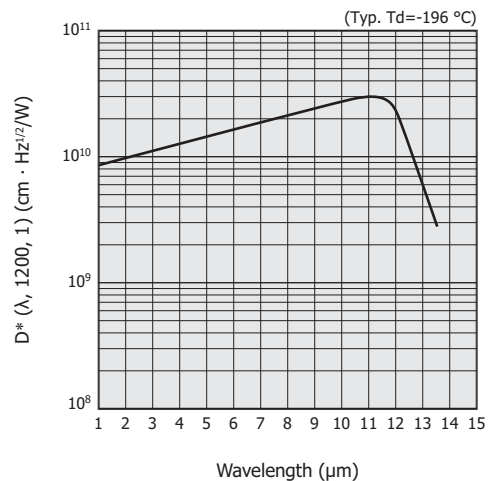
## 8. MCT(HgCdTe) photovoltaic detectors

MCT photovoltaic detectors are infrared detectors utilizing the photovoltaic effect that generates photocurrent when illuminated with infrared light, the same as InAs photovoltaic detectors. These MCT photovoltaic detectors are mainly used for infrared detection around 10  $\mu\text{m}$ .

### 8-1 Characteristics

#### Spectral response

[Figure 8-1] Spectral response (MCT photovoltaic detector)



KIRDB0334EB

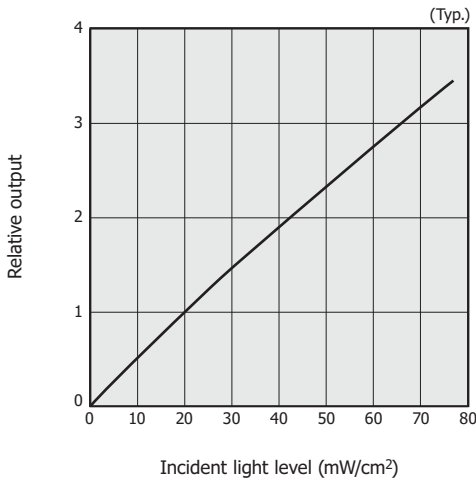
#### Noise characteristics

To find information on photovoltaic detector noise characteristics, see "6-1 Characteristics/Noise characteristics" in section 6, "InAs/InAsSb/InSb photovoltaic detectors." Compared to photoconductive detectors, photovoltaic detectors have smaller  $1/f$  noise and are therefore advantageous for measuring light at low frequencies.

#### Linearity

The upper linearity limit of MCT photovoltaic detectors is one order of magnitude or more higher than that (several  $\text{mW}/\text{cm}^2$ ) of MCT photoconductive detectors.

[Figure 8-2] Linearity (MCT photovoltaic detector)



KIRDB0404EA

## 8 - 2 How to use

### Operating circuit

The connection example for MCT photovoltaic detectors is similar to Figure 6-5. The photocurrent is extracted as a voltage using a load resistor or op amp.

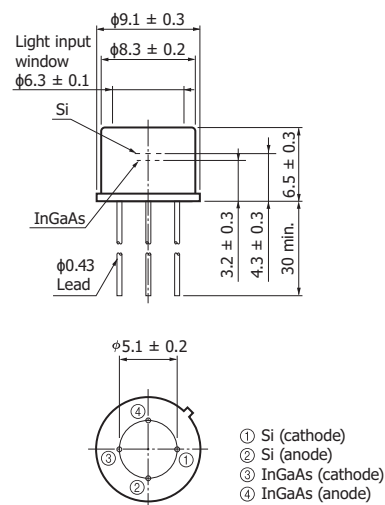
### Ambient temperature

In MCT photovoltaic detector operation, if the background radiation noise changes due to ambient temperature fluctuations, then the dark current also changes. To prevent this phenomenon, pay attention to optical system design. For example use a properly shaped cold shield that does not allow pickup of unnecessary background light.

## 9. Two-color detectors

Two-color detectors are infrared detectors that use two or more vertically stacked detectors to extend the spectral response range. We provide products with a Si photodiode mounted as the light incident surface over a PbS or PbSe or InGaAs detector along the same optical axis as well as products with a standard type InGaAs mounted over a long wavelength type InGaAs. Other combinations such as InAs and InSb or InSb and MCT (HgCdTe) can also be used for the same purpose. The upper detector not only detects infrared light but also serves as a short-wavelength cutoff filter for the lower detector.

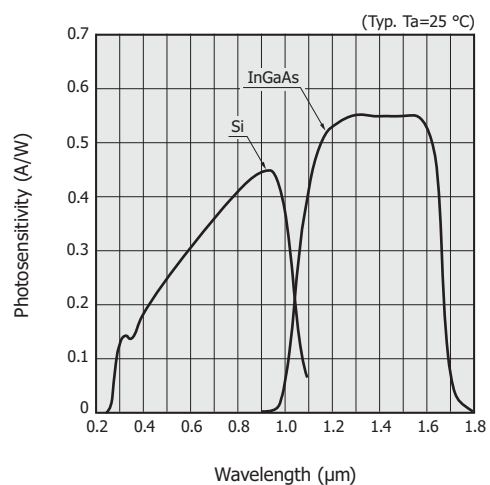
[Figure 9-1] Dimensional outline  
[two-color detector (Si + InGaAs), unit: mm]



KIRDA0147EB

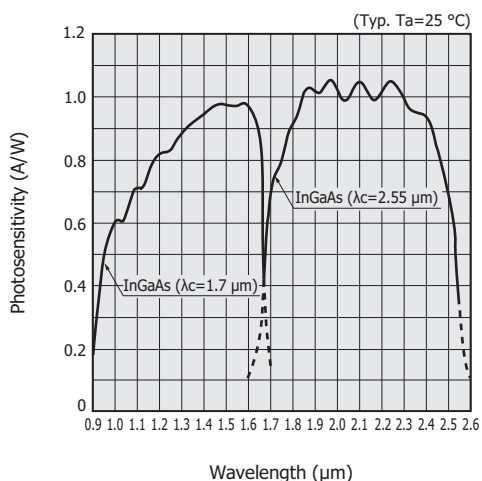
[Figure 9-2] Spectral response

(a) Two-color detector (Si + InGaAs)



KIRDB0405EB

(b) Two-color detector  
(standard type InGaAs + long wavelength type InGaAs)

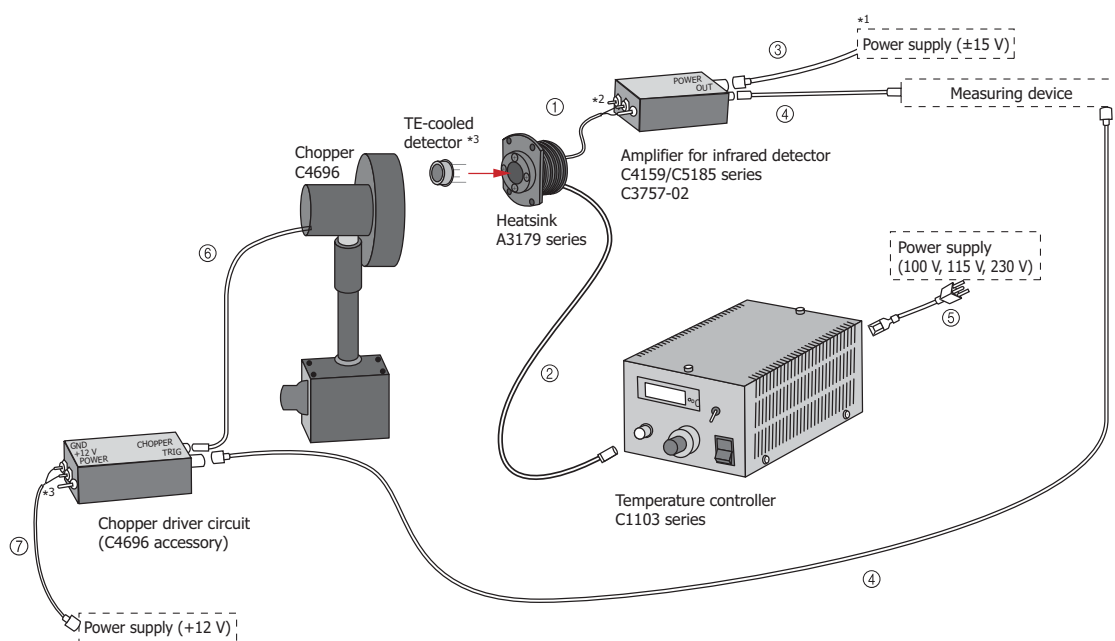


KIRDB0479EB

## 10. Options

Hamamatsu offers amplifiers, temperature controllers, heatsinks, chopper, cables, and the like as compound semiconductor photosensor options. Temperature controllers and heatsinks are for TE-cooled types. Temperature controllers are used to maintain the element temperature at a constant level, and heatsinks are used to radiate heat efficiently from the TE coolers. Choppers can be used to modulate only the detected light to separate it from the background light when performing infrared detection. This helps to reduce the effect of background light. Furthermore, we also provide infrared detector modules with a preamp, which integrates an infrared detector and preamp into a single device.

[Figure 10-1] Connection example of options for compound semiconductor photosensors



KAC00321EC

Cable no.	Cable	Approx. length	Remarks
①	Coaxial cable (for signal)	2 m	Supplied with heatsink A3179 series. Make the cable as short as possible. (About 10 cm is desirable.)
②	4-conductor cable (with a connector) A4372-05	3 m	Supplied with temperature controller C1103 series. It is also sold separately.
③	Power supply cable (with a 4-conductor connector) A4372-02	2 m	Supplied with C4159/C5185 series and C3757-02 amplifiers for infrared detectors and infrared detector modules with preamp (room temperature type). It is also sold separately. Power supply cable (with a 6-conductor connector) A4372-03 [supplied with infrared detector modules with preamp (cooled type)] is also sold separately.
④	BNC connector cable E2573	1 m	Sold separately
⑤	Power supply cable (for temperature controller)	1.9 m	Supplied with temperature controller C1103 series
⑥	Chopper driver cable (connected to chopper)	2 m	Connect to a chopper driver circuit.
⑦	2-conductor cable or coaxial cable (for chopper power supply)	2 m or less	Please provide your own cable.

\*1: Connect unterminated wires or the like to the power supply.

\*2: Soldering is required. A BNC connector is required to use the C5185 series amplifier. (Please provide your own connector. example: one end of the E2573)

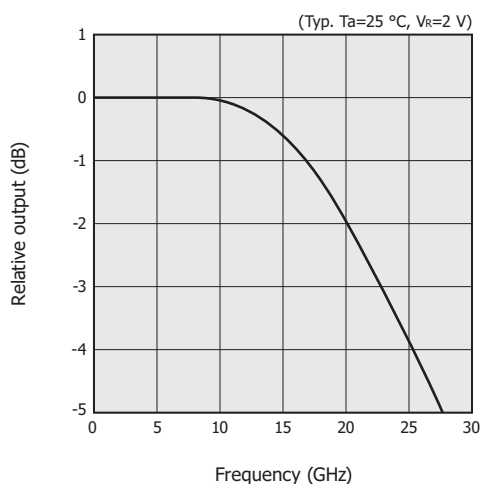
\*3: There is no dedicated socket. Soldering is required.

## 11. New approaches

### 11 - 1 High-speed InGaAs PIN photodiodes

As fast response photosensors, the product demand for 25 Gbps and 40 Gbps photodiodes is on the rise. In this case, it is essential to keep the cost of the system itself from rising, so low power consumption and ease of assembling are required. Moreover, to ensure the S/N, reduction in sensitivity from previous products is not acceptable. The photodiodes must maintain the present photosensitivity and operate at high speed under a low reverse voltage. At the same time, the manufacturing process must integrate optical techniques to guide as much light as possible into a small photosensitive area. We have produced a high-speed InGaAs PIN photodiode that operates from a low reverse voltage and verified its operation on transmission bands up to 25 Gbps at  $V_R=2$  V. We are currently working to achieve even higher speeds.

[Figure 11-1] Frequency characteristics (high-speed InGaAs PIN photodiode)



KIRDB0394EA

### 11 - 2 100 Gbps ROSA modules

Optical communications will continue to achieve higher speeds in the future. Standardization of 40 Gbps Ethernet for data center applications and 100 Gbps Ethernet for metropolitan area networks has been completed as a follow up to the 10 Gbps version. However, sending data serially at 100 Gbps is currently extremely difficult because of the technical level of photodiodes, transimpedance amplifiers, etc., so wavelength division multiplexing methods are being used.

Wavelength division multiplexing of “25 Gbps × 4 ch” is employed for 10 km and 40 km transmissions over single-mode fibers.

The 1310 nm wavelength band is being used since there is little dispersion. Externally or directly modulated four wavelengths of laser light are multiplexed and transmitted in a single-mode fiber.

In the 40 km version, an SOA (semiconductor optical amplifier) or the like is used on the receiving side to boost the power of the light being received.

The transmission method of “25 Gbps × 4 ch” not only uses devices operating at higher speeds than before, but also requires using wavelength division multiplexing technology. Hamamatsu is developing photodiodes and modules that can handle these high speeds. Photodiode structures and other factors were reviewed to develop a 4 ch photodiode array with preamps that can be used at 25 Gbps per channel [Figure 11-2]. Silicon is used for the package material. The package is hermetically sealed to ensure high reliability. It has a flexible cable to make it easy to connect to the latter-stage circuit. Inside the package are impedance-optimized patterning for handling high frequencies, photodiode array, and amplifiers. To achieve multichannel devices for wavelength division multiplexing, we are working to develop 100 Gbps ROSA modules that integrate optical splitting functions.

[Figure 11-2] 4 ch photodiode array with preamp (100 Gbps)

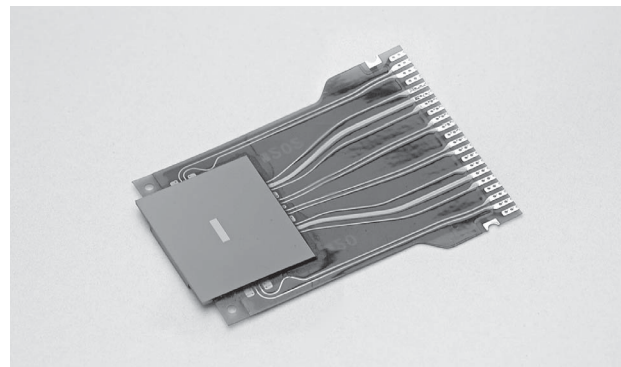
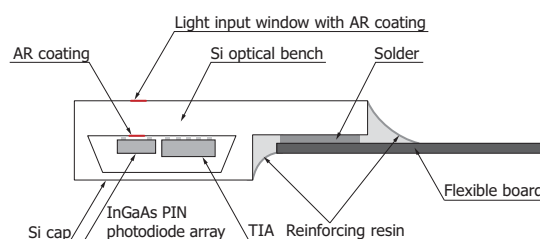


[Figure 11-3] Cross section (4 ch photodiode array with preamp)



KACCC0717EA

### 11 - 3 InAsSb photovoltaic detectors

The infrared region is drawing much attention in many fields, but there are only few easy-to-use detectors available. Hamamatsu has studied semiconductor materials with high crystal uniformity and that can be fabricated into large-area devices and has chosen InAsSb, a III-V family compound semiconductor. Controlling the composition of InAs<sub>x</sub>Sb<sub>1-x</sub> enables the fabrication of detectors whose cutoff wavelength at room temperature ranges from 3.3 μm (InAs) to 12 μm (InAs<sub>0.38</sub>Sb<sub>0.62</sub>). We are currently developing a TE-cooled 10 μm-band type. We are also actively engaged in developing devices that will detect even longer wavelengths as well as one-dimensional and two-dimensional arrays.

[Figure 11-4] Band gap energy and peak sensitivity wavelength vs. composition ratio x of InAs<sub>x</sub>Sb<sub>1-x</sub>

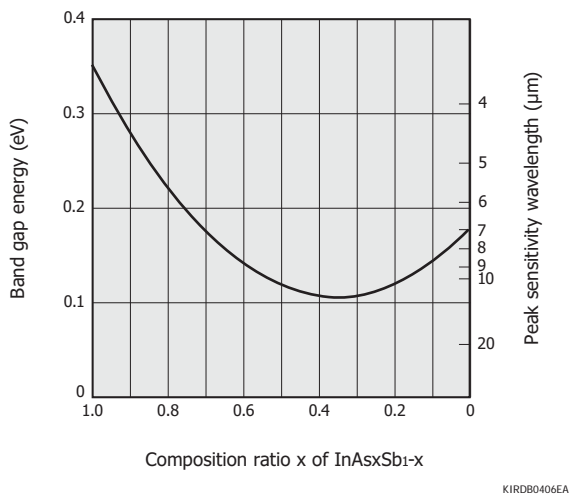
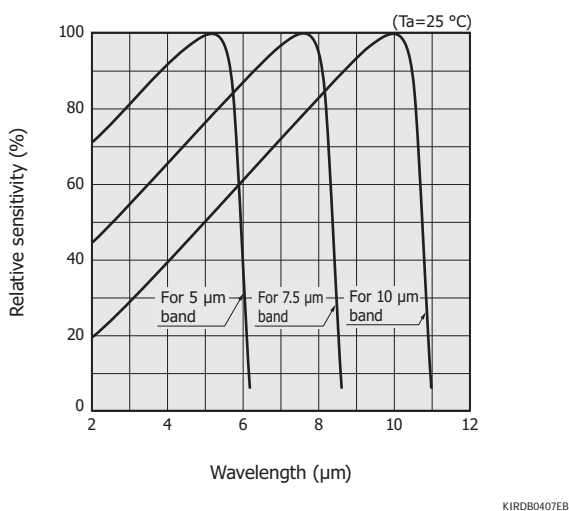


[Figure 11-5] Spectral response (InAsSb photovoltaic detectors, typical example)



## 12. Applications

### 12 - 1 Optical power meters

Optical power meters measure light level and are used in a wide range of applications including optical fiber communications and laser beam detection. Optical fiber communications are grouped into two categories: short/middle distance and long distance communications. In long distance communications, infrared light in the 1.3 and 1.55 μm wavelength regions, which has less optical loss during transmission through optical fibers, is used. In these wavelength regions, InGaAs PIN photodiodes are used to measure transmission loss in optical fibers, check whether relays are in satisfactory condition, and measure laser power. Major characteristics required of optical power meters are linearity and uniformity. In some cases, cooled type detectors are used to reduce the noise levels so that even low-power light can be detected.

[Figure 12-1] Optical power meter

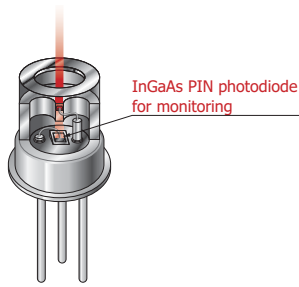


### 12 - 2 LD monitors

The output level and emission wavelength of LD (laser diodes) vary with the LD temperature. So APC (automatic power control) is used to stabilize the LD. APC includes two methods. One method monitors the integrated amount of light pulses from the LD, and the other monitors the peak values of light pulses. Along with the steady increase in LD output power, linearity at higher light levels has become important for the detectors used in these monitors. High-speed response is also required to monitor the peak values of light pulses.

InGaAs PIN photodiodes used for LD monitors are mounted either in the same package as the LD or outside the LD package. Also, InAs and InSb photovoltaic detectors are used to monitor lasers at even longer wavelengths.

[Figure 12-2] LD monitor



K1RDC0096EB

## 12 - 3 Radiation thermometers

Any object higher than absolute zero degrees radiates infrared light matching its own temperature. The quantity of infrared light actually emitted from an object is not directly determined just by the object temperature but must be corrected according to the object's emissivity (e).

Figure 12-3 shows the radiant energy from a black body. The black body is e=1. Figure 12-4 shows the emissivity of various objects. The emissivity varies depending on temperature and wavelength.

The noise equivalent temperature difference (NEΔT) is used as one measure for indicating the temperature resolution. NEΔT is defined in equation (1).

$$NE\Delta T = \frac{L_N}{\left. \frac{dL}{dT} \right|_{T=T_1}} \dots\dots (1)$$

$L_N$ : noise equivalent luminance  
 $T_1$ : temperature of object

Noise equivalent luminance ( $L_N$ ) relates to the detector NEP as shown in equation (2).

$$NEP = T_0 L_N \Omega A_o / \gamma \dots\dots (2)$$

$T_0$ : optical system loss  
 $\Omega$ : solid angle from optical system toward measurement area  
 $A_o$ : aperture area of optical system  
 $\gamma$ : circuit system loss

$\left. \frac{dL}{dT} \right|_{T=T_1}$  in equation (1) represents the temperature coefficient of radiant luminance (L) from an object at temperature  $T_1$ . The radiant luminance can be obtained by integrating the spectral radiant exitance over the wavelength range ( $\lambda_1$  to  $\lambda_2$ ) being observed.

$$L = \int_{\lambda_1}^{\lambda_2} \frac{1}{\pi} M_\lambda d\lambda \dots\dots (3)$$

$M_\lambda$ : spectral radiant exitance

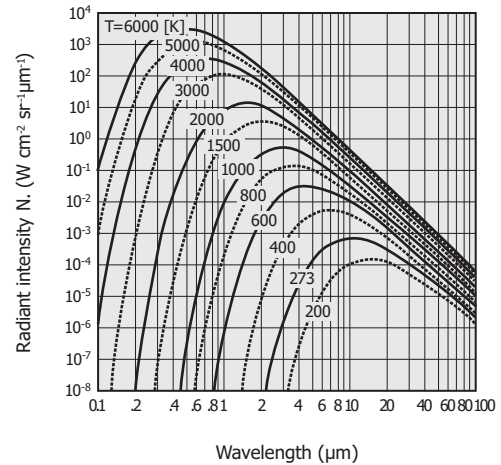
Radiation thermometers offer the following features compared to other temperature measurement methods.

- Non-contact measurement avoids direct contact with object.
- High-speed response
- Easy to make pattern measurements

Infrared detectors for radiation thermometers should be selected according to the temperature and material of the object to be measured. For example, peak emissivity wavelength occurs at around 5  $\mu\text{m}$  in glass materials and around 3.4  $\mu\text{m}$  or 8  $\mu\text{m}$  in plastic films, so a detector sensitive to these wavelength regions must be selected.

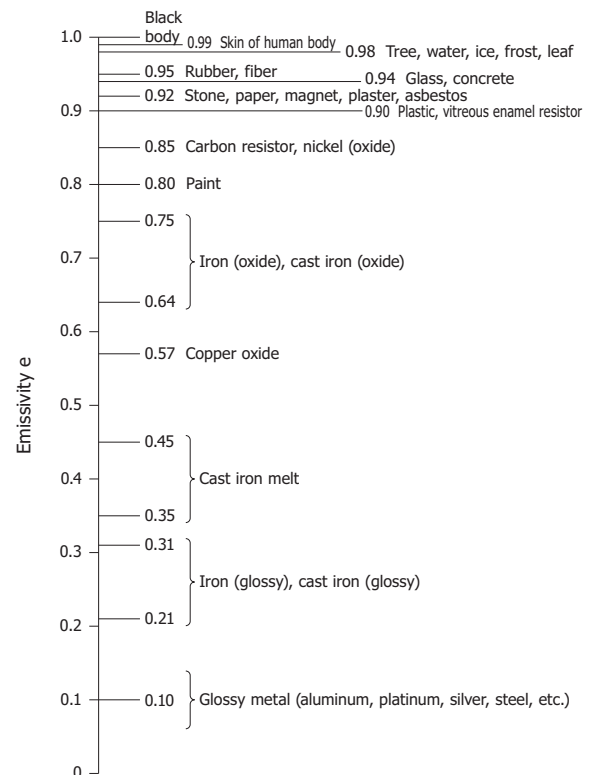
Infrared detectors combined with an infrared fiber now make it possible to measure the temperature of objects in hazardous locations such as hot metal detectors (HMD), rotating objects, complex internal structures, and objects in a vacuum or in high-pressure gases.

[Figure 12-3] Black body radiation law (Planck's law)



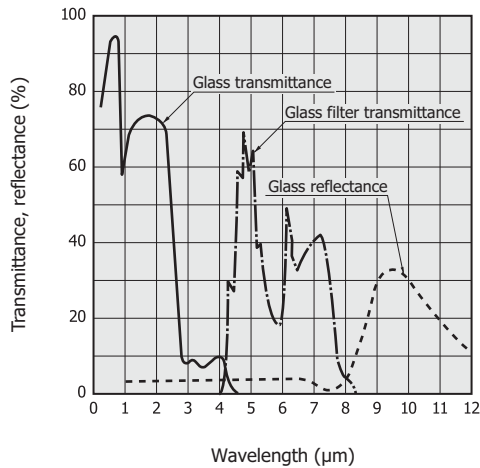
K1RDB0014EB

[Figure 12-4] Emissivity of various objects



K1RDC0036EA

[Figure 12-5] Spectral transmittance and reflectance of glass

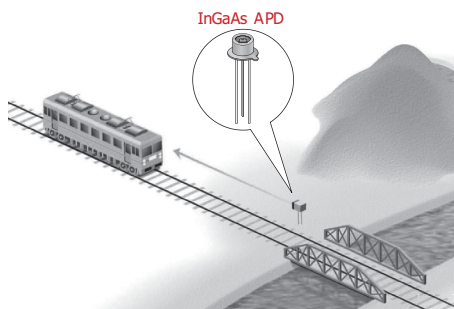


KIRDB0146EA

## 12 - 4 Distance measurement

Distance to a target object can be measured at high speeds and high accuracy by directing a laser beam at the target object and detecting the reflected low-level light. The InGaAs APD achieves high S/N when it is applied with a reverse voltage and is suitable for low-level-light measurement, so it is often used as a distance sensor.

[Figure 12-6] Distance measurement

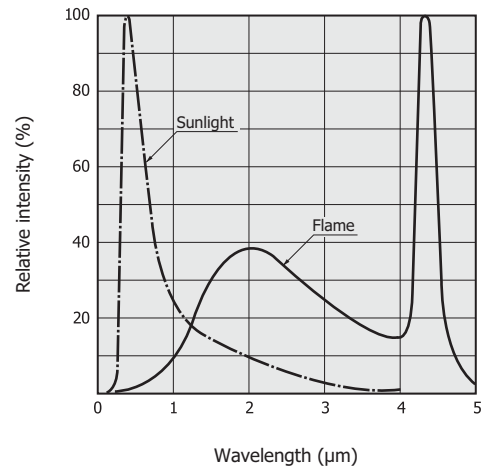


KIRDC0098EA

## 12 - 5 Flame eyes (flame monitors)

Flame monitors detect light emitted from flames to monitor the flame burning state. Radiant wavelengths from flames cover a broad spectrum from the ultraviolet to infrared region as shown in Figure 12-7. Flame detection methods include detecting infrared light using a PbS photoconductive detector, detecting a wide spectrum of light from ultraviolet to infrared using a two-color detector (Si + PbS), and detecting the 4.3 μm wavelength using a PbSe photoconductive detector.

[Figure 12-7] Radiant spectrum from flame



KIRDB0147EA

## 12 - 6 Moisture meters

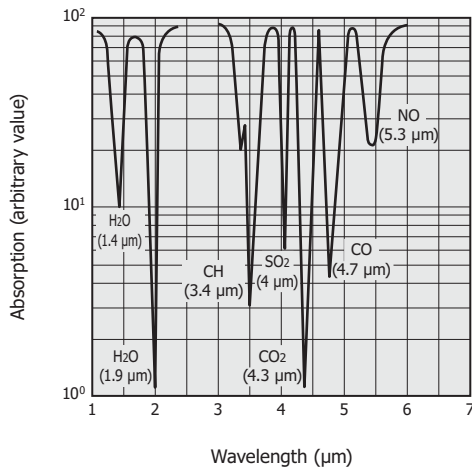
Moisture meters measure the moisture of objects such as food by illuminating the object with reference light and with near infrared light at water absorption wavelengths (1.1 μm, 1.4 μm, 1.9 μm, 2.7 μm). The two types of light reflected from or transmitted through the object are detected, and their ratio is calculated to measure the moisture level of the object. Photosensors suited for moisture measurement include InGaAs PIN photodiodes, InAs photovoltaic detectors, and PbS photoconductive detectors.

## 12 - 7 Gas analyzers

Gas analyzers measure gas concentrations by making use of the fact that gases absorb specific wavelengths of light in the infrared region. Gas analyzers basically utilize two methods: a dispersive method and a non-dispersive method. The dispersive method disperses infrared light from a light source into a spectrum and measures the absorption amount at each wavelength to determine the constituents and quantities of the sample. The non-dispersive method measures the absorption amounts only at particular wavelengths. The non-dispersive method is currently the method mainly used for gas analysis. Non-dispersive method gas analyzers are used for measuring automobile exhaust gases (CO, CH, CO<sub>2</sub>) and exhaled respiratory gas components (CO<sub>2</sub>), as well as for regulating fuel exhaust gases (CO<sub>x</sub>, SO<sub>x</sub>, NO<sub>x</sub>) and detecting fuel leaks (CH<sub>4</sub>, C<sub>2</sub>H<sub>6</sub>). Further applications include CO<sub>2</sub> (4.3 μm) measurements in carbonated beverages (soft drinks, beer, etc.) and sugar content (3.9 μm) measurement. Figure 12-8 shows absorption spectra of various gases.

Hamamatsu provides InGaAs, InAs, InAsSb, InSb, PbS, PbSe, MCT, and the like, as sensors to measure the various light wavelengths. Quantum cascade lasers (QCL; middle infrared semiconductor lasers) are also available for use in gas analyzers. There is a lineup of products with specific oscillation wavelength in the middle infrared region (4 to 10 μm).

[Figure 12-8] Gas absorption spectra



KIRDB0148EA

## 12 - 8 Infrared imaging devices

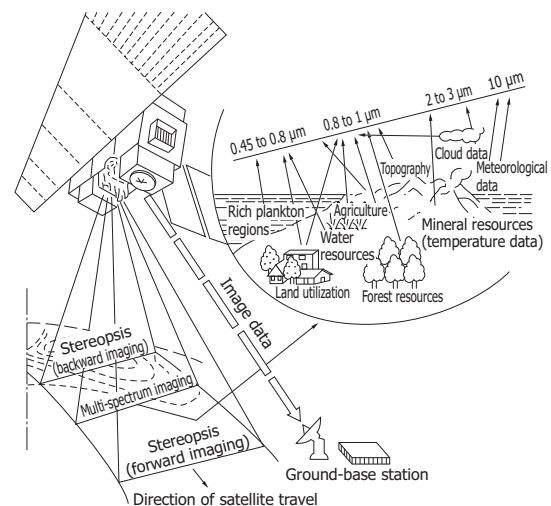
Infrared imaging devices are finding a wide range of applications from industry to medical imaging, academic research, and many other fields [Table 12-1]. The principle of infrared imaging is grouped into two techniques. One technique uses a one-dimensional array as a detector and captures an image by scanning the optical system from the Z axis. The other technique uses a two-dimensional array and so does not require scanning the optical system. Even higher quality images can be acquired with InSb or MCT photoconductive/photovoltaic detectors, QWIP (quantum well infrared photodetector), thermal detectors utilizing MEMS technology, and two-dimensional arrays fabricated by heterojunction to CMOS circuitry.

## 12 - 9 Remote sensing

Light emitted or reflected from objects contains different information depending on the wavelength as shown in Figure 12-9. Measuring this light at each wavelength allows obtaining various information specific to the object. Among the various measurements, infrared remote sensing can acquire information such as the surface temperature of solids or liquids, or the type and temperature of gases. Remote sensing from space satellites and airplanes is recently becoming increasingly used to obtain global and macroscopic information such as the temperature of the earth's surface or sea surface and the gas concentration in the atmosphere. Information obtained in this way is utilized for environmental measurement, weather observation, and resource surveys.

MTC/InSb arrays are used to measure the temperature of the earth's surface or sea surface, and MCT is used to detect the gas concentration in the atmosphere.

[Figure 12-9] Optical system for resource survey



KIRDC0039EB

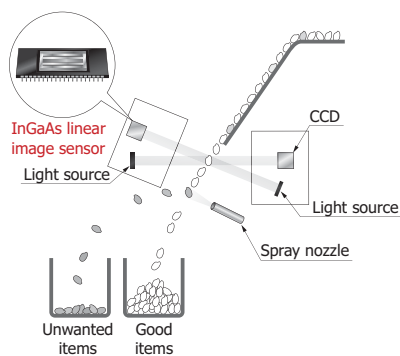
[Table 12-1] Infrared imaging device application fields

Application field	Applications
Industry	Process control for steel and paper, non-destructive inspection of welds or soldering, non-destructive inspection of buildings and structures, evaluating wafers and IC chips, inspecting and maintaining power transmission lines and electric generators, heat monitoring of shafts and metal rolling, marine resource surveys, forest distribution monitoring
Pollution monitor	Monitoring of seawater pollution and hot wastewater
Academic research	Geological surveys, water resource surveys, ocean current research, volcano research, meteorological investigations, space and astronomical surveys
Medical imaging	Infrared imaging diagnosis (diagnosis of breast cancer and the like)
Security and surveillance	Monitoring of boiler temperatures, fire detection
Automobile, airplane	Night vision device for visual enhancement, engine evaluations

## 12 - 10 Sorting machines

Making use of the absorption wavelengths inherent to organic matter allows sorting it into organic and inorganic matter. Agricultural crops such as rice, potatoes, tomatoes, onions, and garlic are distinguished from clods and stones based on this principle by using InGaAs PIN photodiode arrays and PbS photoconductive detectors. These infrared detectors also detect differences in temperature, emissivity, and transmittance of objects carried on a conveyor in order to sort fruits for example by sugar content or to separate waste such as plastic bottles for recycling.

[Figure 12-10] Grain sorting by detecting transmitted light



KIRD0099EA

## 12 - 11 FT-IR

The FT-IR (Fourier transform-infrared spectrometer) is an instrument that acquires a light spectrum by Fourier-transforming interference signals obtained with a double-beam interferometer. It has the following features:

- High power of light due to non-dispersive method (simultaneous measurement of multiple spectral elements yields high S/N)
- High wavelength accuracy

The following specifications are required for infrared detectors that form the core of the FT-IR.

- Wide spectral response range
- High sensitivity
- Photosensitive area size matching the optical system
- Wide frequency bandwidth
- Excellent linearity versus incident light level

Thermal type detectors are generally used over a wide spectral range from 2.5  $\mu\text{m}$  to 25  $\mu\text{m}$ . Quantum type detectors such as MCT, InAs, and InSb are used in high-sensitivity and high-speed measurements.

Usage of InGaAs and InAs has also extended the spectral range to the near infrared region. One-dimensional or two-dimensional arrays such as MCT and InSb are used for infrared mapping and infrared imaging spectrometry.